RAMAN SCATTERING STUDIES

Richard L. St. Peters, et al

General Electric Corporate Research and Development

Prepared for:

Advanced Research Projects Agency
Office of Naval Research

28 February 1973

GENERAL ELECTRIC

GENERAL ELECTRIC COMPANY
CORPORATE RESEARCH AND DEVELOPMENT
Schenectady, N.Y.

RAMAN SCATTERING STUDIES

Final Technical Report: Contract No. N00014-72-C-0503
Contract Period: 15 April 1972 to 31 December 1972
Amount: $103,184

Sponsored by: Advanced Research Projects Agency
ARPA Order No. 1806, Amendment 2
Program Code 421

Principal Investigator: Dr. Donald R. White
(518) 377-3136

Contractor: General Electric Company
Corporate Research and Development
Schenectady, New York 12301

Scientific Officer: Director, Physics Program
Physical Sciences Division
Office of Naval Research
Department of the Navy
800 North Quincy Street
Arlington, Virginia 22217

February 1973

SRD-73-033

unclassified

Security Classification

DOCUMENT CONTROL DATA - R & D

Security classification of title, body of abstract and indexing annotation must be entered when the overall report is classified)

1. ORIGINATING ACTIVITY (Corporate author) General Electric Company Corporate Research and Development P.O. Box 8, Schenectady, New York 12301	2a. REPORT SECURITY CLASSIFICATION unclassified 2b. GROUP

3. REPORT TITLE

Raman Scattering Studies

4. DESCRIPTIVE NOTES (Type of report and inclusive dates)

Final Technical Report 72 Apr. 15 - 72 Dec. 31

5. AUTHOR(S) (First name, middle initial, last name)

Richard L. St. Peters, Seth D. Silverstein, William W. Morey, David J. Taylor

6. REPORT DATE 26 February 1973	7a. TOTAL NO. OF PAGES 87 104	7b. NO. OF REFS 34
8a. CONTRACT OR GRANT NO N00014-72-C-0503 b. PROJECT NO c d.	9a. ORIGINATOR'S REPORT NUMBER(S) SRD-73-033 9b. OTHER REPORT NO(S) (Any other numbers that may be assigned this report)	

10. DISTRIBUTION STATEMENT

11. SUPPLEMENTARY NOTES This program has been monitored by the Physical Sciences Division, Office of Naval Research	12. SPONSORING MILITARY ACTIVITY Advanced Research Projects Agency 1400 Wilson Boulevard Arlington, Virginia 22209

13. ABSTRACT

Absolute cross sections for rotational Raman scattering have been derived for N_2 and O_2 from the near uv to the IR, with particular attention to 10.6μ, using a theoretical extrapolation of data obtained in the visible.

The feasibility of remote optical sensing using near resonant enhancement of Raman scattering has been studied by a search for such enhancement from ClF, Cs_2, and Na_2. Enhancement was seen from Na_2, but the signal could not be clearly demonstrated as Raman scattering.

Use of resonant effects (Raman, fluorescence, or absorption) in remote probing requires both a narrow line and high power from a tunable laser. Injection narrowing of a high power flashlamp-pumped oscillator is shown to be an effective means to obtain a narrow line at reasonable power. Application of the Zig-Zag Face-Pumped laser configuration to dye lasers is shown to provide a high brightness, high average power amplifier, and a design basis for further development has been established.

DD FORM 1 NOV 1473

unclassified

Security Classification

KEY WORDS	LINK A		LINK B		LINK C	
	ROLE	WT	ROLE	WT	ROLE	WT
Raman scattering						
rotational Raman scattering						
resonance Raman scattering						
tunable laser						
dye laser						
injection narrowing						
Zig-Zag Face-Pumped Laser						

TABLE OF CONTENTS

RAMAN SCATTERING STUDIES

R. L. St. Peters, S. D. Silverstein, W. W. Morey, and D. J. Taylor

Optical Physics Branch
General Electric Corporate Research and Development

SUMMARY

Rotational Raman scattering cross sections for N_2 and O_2 in the infra-red are desired for analysis of the propagation of high power laser radiation through the atmosphere, particularly at 10.6 μ. While direct measurement of these cross sections is difficult due both to their small values and to experimental problems, accurate measurements are available at visible wavelengths. The theory necessary to extrapolate these data is developed, and tabulated cross sections for rotational Raman scattering are presented from 265 nm in the uv to 10.6 μm in the IR. Since N_2 and O_2 are homonuclear diatomic molecules with no IR absorption, extrapolation across absorption bands is not necessary, and the accuracy is expected to be high. This work is described in detail in Appendix A.

Since the scattered wavelength in Raman scattering is shifted from the incident wavelength by an amount characteristic of and dependent on the scattering species, Raman scattering is attractive as a non-sampling technique for gas analysis. Theory suggests that this normally weak phenomenon can be strongly enhanced by the use of incident wavelengths which are tuned to be near but not on an absorption line of the scattering species. If this enhancement is realizable, then resonance Raman scattering offers an approach to remote measurement in the atmosphere of molecules of military significance. The small tuning range of presently available lasers with adequate wavelength control limited our laboratory investigation of this enhancement to a few species. In one, Na_2 vapor, evidence of a resonant Raman return signal was found but a clear demonstration of its Raman-like character was not possible within the scope of this work. If the observed signal is resonant Raman scattering rather than fluorescence, it corresponds to an enhancement of roughly 10^7 over ordinary

Raman scattering. The other two species investigated, Cs_2 vapor and ClF gas, proved unsuitable for these resonant Raman scattering studies.

Near resonance Raman scattering is only one of several approaches to remote optical probing; others including absorption of Raman backscatter from N_2 and of Rayleigh backscatter. All such remote probing techniques with high sensitivity depend on the availability of high pulse energy tunable lasers. The most promising type of tunable laser is the dye laser, but effective use of a dye laser requires narrowing of its normally broad spectral output, and then tuning of this narrow spectrum to the desired wavelength. Conventional narrowing techniques involve dispersive cavity elements with significant insertion loss, resulting in substantial power loss. However, if a low power, spectrally narrow beam is injected into the laser cavity before oscillation begins, the laser's output spectrum is locked to the injected spectrum without loss of power. In this program an injected power of 11 watts, for example, is found to be sufficient to narrow a several hundred kilowatt laser. The beam to be injected is readily obtained from a low power dye laser which can be easily narrowed by conventional means. Details of this work are in Appendix C.

High power dye lasers are of potential interest not only in remote probing applications, but also for example for underocean use. In the latter case the wavelength match to the ocean window and the high peak power are relevant, the narrow spectrum and tunability are not. Such high pulse energy dye lasers however have been limited to low repetition rates, one pulse every few seconds at best, due to thermally-induced distortion in the laser cavity. A dye Zig-Zag Face-Pumped Laser configuration, designed to eliminate this distortion, was found to introduce no detectable distortion into a He/Ne probe beam while operating at an average power of 1 kW into the flashlamps. Using unpurified commercial dye and no special quenchants, an average output power of over one watt was obtained at three pulses per second. This limit was imposed by difficulties with the flashlamp triggering at higher repetition rates, not by thermal distortion. Performance analysis indicates substantial performance improvements can be obtained by straightforward design changes. The projected performances of one proposed design are given for both oscillator and amplifier use. Studies on the dye Zig-Zag-FPL are given in Appendix D.

RAMAN SCATTERING STUDIES

I. INTRODUCTION

Raman scattering from molecular gases is a process in which a small fraction of light energy incident on a gas is scattered by that gas, with the wavelength of the scattered light shifted from the wavelength of the incident light. The wavelength shift is different for different gases, and the scattering at each gas' characteristic wavelength is proportional to the density of that gas and independent of the densities of any other gases present. Thus Raman scattering can be used to probe for the presence of one or more species of interest in a mixture of gases. Although Raman scattering is normally a very weak process, enhancement of the scattering cross section by proximity of the incident wavelength to an absorption line of the scattering species is expected. Utilization of this enhancement requires a light source which can be tuned to an appropriate wavelength for each species of interest.

In Raman scattering processes, a gas molecule simultaneously absorbs an incident photon and emits a scattered photon while undergoing a change in its internal excitation energy. The energy difference between scattered and incident photons equals the energy difference between the initial and final states of the molecule. In general, scattering occurs at a number of shifted wavelengths with the energy shifts corresponding to energy level spacings of the molecule. There are two general categories of Raman scattering of interest: 1) rotational Raman scattering, in which the molecule changes its rotational energy, and 2) vibrational Raman scattering in which the molecule changes its vibrational state. A third category, in which the molecule changes both its rotational and vibrational states, is so weak that it is seldom of interest.

Rotational energy level spacings in molecules are usually small and therefore the wavelength shifts in rotational Raman scattering are small. The selection rule $\Delta J = \pm 2$ permits molecules in states with $J \geq 2$ to scatter at two wavelengths. In one case, $\Delta J = +2$, the molecule is left in a higher rotational energy level and the scattered photon energy is less. The scattered wavelength is thus longer than the incident wavelength (stokes scattering).

For the $\Delta J = -2$ process the scattered wavelength is shorter (antistokes scattering). These two scattering processes from rotational states low enough to be significantly populated yield a series of nearly equally spaced scattered wavelengths extending about two or three nm (for the visible wavelength region) on either side of the incident wavelength. After the first few lines the intensity falls off rapidly.

Vibrational energy level spacings are usually much larger than the rotational spacings, and at ambient temperatures only the vibrational ground state is normally occupied. Only $\Delta v = \pm 1$ processes are allowed and of course only $\Delta v = +1$ can occur from the ground state. Scattering processes raising the molecule to a vibrationally excited state yield a scattered wavelength shifted toward longer wavelength by an amount depending on the vibrational state separation. Shifts as large as 100 nm occur for the visible wavelength region; polyatomic molecules with more than one vibrational mode yield multiple scattered wavelengths. Since the rotational spacings are nearly the same for the upper and lower vibrational states, these scattered wavelengths are nearly independent of the rotational state. The vibrational Raman spectrum thus consists of one scattered wavelength for each vibrational mode.

The work in this program was divided into three tasks. The first consisted of a theoretical extrapolation of rotational Raman scattering cross sections for N_2 and O_2 across the spectrum from the far infra-red to the ultraviolet, based on measurements in the visible. This calculation takes into account the frequency dependence of the polarizability. The second task was an attempt to find and evaluate resonance enhancement of Raman scattering from a few molecules whose absorption is within the very narrow tuning range of existing ion lasers. The spectral coincidences which are necessary severely limited the choice of molecules, and this effort was essentially unsuccessful. In the third task substantial progress was made toward a high power tunable laser with a sufficiently narrow linewidth to be useful as a source for remote optical probes based on resonance enhancement.

II. ABSOLUTE ROTATIONAL RAMAN SCATTERING CROSS SECTIONS

The wavelength dependence of Raman cross sections is often taken to be $(1/\lambda_R)^4$ where λ_R is the scattered wavelength. This is only an approximation, however, and for high accuracy or for extrapolation over large wavelength

intervals the wavelength dependence of the polarizability, which leads to more complex wavelength dependence, must be taken in consideration. The wavelength dependence of the polarizability is related to the molecule's absorption bands. In this work the theory is developed adequately to extrapolate rotational Raman cross sections from the uv to the far IR for molecules which do not have any IR absorption (i.e., homonuclear diatomic molecules such as O_2 and N_2). Coupled with absolute cross section measurements for rotational Raman scattering from N_2 and O_2 at 488 nm, the theory yields absolute cross sections over the same wavelength range. These results for N_2 and O_2 are tabulated for four incident wavelengths from 265 nm to 10.6 um in Ref. 1 which is included here as Appendix A. This appendix also gives the development of the theory culminating in an expression which can be used for other molecules with no IR absorptions.

III. RESONANT ENHANCEMENT OF RAMAN SCATTERING

Enhancement of Raman scattering due to proximity of the incident wavelength to a single isolated absorption line of the scattering species was the principal interest in this task. If the incident wavelength is too close, or if the incident linewidth overlaps the absorption line, then absorption of the incident power will occur. This absorption will be followed by fluorescence; the fluorescence occurs at the same wavelengths as the Raman scattering. Although much stronger than resonant Raman scattering, fluorescence is not as useful since its intensity may be strongly affected by other gases present due to collision quenching processes. Thus a narrow, tunable source is required to avoid fluorescence and obtain resonant Raman scattering.

Ion lasers can be operated single-mode and tuned within the gain bandwidths of their available lines. In this manner an argon or krypton ion laser can operate with a bandwidth of $< 10^{-4}$ nm tuned over several ion lines in the visible, each line $\sim 10^{-2}$ nm wide. Use of such a source limits the molecules suitable for resonance studies to those with the necessary spectral coincidences; we investigated three such molecules: ClF, Cs_2, and Na_2.

We found that the absorption transitions of ClF have transition probabilities which are too small to contribute measureable enhancement. The absorption spectrum of Cs_2 consists of lines which are too closely spaced to isolate the effects of any single line.

Sodium molecules, Na_2, appear well suited to resonance studies except for the experimental difficulties associated with reactive metal vapors. With the laser tuned off an isolated Na_2 absorption line by 135-200 linewidths (of the absorption line) we observed a signal which was roughly 10^7 larger than ordinary Raman scattering would be. However, we were unable to demonstrate that this signal has the character of Raman scattering rather than fluorescence, due to the difficulty of the necessary experiments. With more effort than was possible in this work such a demonstration can probably be made using Na_2. The details of our investigation are given in Ref. 2 which is included here as Appendix E.

As part of the program in resonant Raman scattering, a theoretical investigation of the non-linear suppression of scattering due to high beam power in the approach to resonance was undertaken.

In the study, we considered the scattering from a single molecule for which we assumed a single quantum model of three levels. Such a model is germane to real molecular systems providing the laser source is close enough to an individual molecular absorption line to effectively isolate the contributions of that line. The problem as posed is soluble, but proved rather difficult in both formulation and solution as it involved extensive use of field theoretic renormalization theory with the evaluation of coupled, self consistent integral equations. The problem couples the sources of the two level quantum self-induced transparency problem with the added complication of Raman channels.

We have been successful in understanding the formal approach and have proceeded towards a formal solution. However, due to the complexity of the problem, more time would have been necessary to reach the solution than was originally anticipated. Completing this effort would have required sacrificing part of the theoretical work directed to scattering at 10.6 μm, which was considered more important.

There are two qualitative conclusions we can draw from our study prior to completion. First, in a real gas, atmospheric-pressure-type environment, pressure broadening effects should act to reduce the non-linear effects. Also, the most significant power effect will not be the "single molecule self-induced transparency", but rather the self-induced transparency effect caused by depletion of the lower molecular state in the absorption process.

IV. TUNABLE LASER DEVELOPMENT

The most promising candidate for a wide-range tunable laser in the visible is the dye laser. For most dyes these lasers have optical gain over a wavelength interval several tens of nm wide, and the entire visible portion of the spectrum plus parts of the uv and IR can be covered using a number of dyes. This property simultaneously allows operation over a wide range of wavelengths and makes operation with a narrow linewidth difficult. The active medium is an organic dye in a liquid solution; this solution is very susceptible to thermally-induced optical inhomogeneities and the resulting distortion at high average power operation. In this work we investigated one promising technique for narrowing the emission linewidth, and we evaluated the performance of a dye laser configuration designed to overcome the distortion difficulties. We found that the line narrowing technique gives excellent results and the low distortion design works very well indeed.

The most direct means of narrowing the linewidth of a dye laser is to introduce into the cavity dispersive elements which have large losses at the undesired wavelengths. At higher pump input levels larger losses are necessary, and line narrowing becomes difficult. Furthermore, the dispersive elements have some loss at the desired wavelength and reduce the output. This technique is thus not suitable for high power operation. In this work we investigate a technique in which a narrow-linewidth low power beam is injected into the high power dye laser cavity before the pump pulse begins. When the flashlamp pump pulse rises above the threshold pump power, the high power laser oscillation which builds up is locked to the injected beam with its narrow linewidth. Little injected power is needed and can be supplied, as in this work, by another dye laser operated at low power where line narrowing is easy. We found that an injected power of 11 watts peak is sufficient to narrow the near-one-megawatt peak power of our high power laser to the injected linewidth. We emphasize that the high power laser is not an amplifier but is a second oscillator; operation as an amplifier would require larger power from the first oscillator for efficient operation. Details of this work are given in Ref. 3 which is included here as Appendix C.

The configuration for eliminating thermal distortion which we investigated in this work is based on a General Electric design, the Zig-Zag Face-Pumped

Laser, which was originally developed to reduce thermal distortion in Nd: glass lasers. Rather than attempt to eliminate all thermal inhomogeneities, this design instead uses face pumping to assure that each optical ray propagating parallel to the axis within the laser aperture traverses the same inhomogeneities, and a high degree of internal self-compensation for the thermal effects is automatically obtained. We operated a dye Zig-Zag Face-Pumped Laser with various values of design parameters to determine the optimum values, measured its performance, and demonstrated its low-distortion properties. We were unable to observe any distortion and achieved an average output power of over 1 watt at three pulses per second. The dye solution was Rhodamine 6G in ethanol at 10^{-3}M, and the output wavelength was 595 nm. An analysis is presented which agrees with the measured performance and can be used to calculate the expected performance of future designs. While the efficiency of this present version is only 0.04%, this can be readily improved by straightforward design modifications. Details are in Ref. 4 which is included here as Appendix D.

V. REMOTE DETECTION OF THE OH RADICAL

As an example which illustrates the potential capabilities of remote probing systems using tunable lasers, we consider the problem of detecting OH^- in a rocket exhaust one meter in diameter at $3000^\circ K$ with a 1% OH^- concentration. We consider two techniques, one based on Raman scattering and the second based on absorption of returned Rayleigh scattering, and we consider detection at a range of 100 km.

The number N of scattered photons collected by the receiving optics, of solid angle Ω, per laser pulse of energy E is

$$N = \frac{E\, \varkappa\, \ell\, \sigma\, \Omega\, T_L\, T_S}{h\, \nu}$$

where $\varkappa$ is the density of scatterers, ℓ is the scattering length, σ is the scattering cross section, $h\nu$ is the scattered photon energy, T_L is the atmospheric transmission at the laser wavelength, and T_S is the transmission at the scattered wavelength.

The OH^- radical has a prominent absorption band near 306.4 nm. Let us take our incident wavelength here; the scattered wavelength is then 344.0 nm. Then, taking

$E = 1$ J,

$\varkappa = 2.5 \times 10^{16}$ molecules/cm^3,

$\ell = 1$ m,

$\Omega = 6.3 \times 10^{-12}$, assuming a 1 meter diameter collection aperture,

$\sigma \approx 4.2 \times 10^{-30}$ cm^2, assuming $\sigma_{OH} \approx \sigma_{N_2}$, and

$h\nu = 5.8 \times 10^{-19}$ J.

Then

$$N = 1.1 \times 10^{-4} T_L T_S \text{ photons per pulse.}$$

If we assume an enhancement of 10^6, then

$$N = 110\, T_L T_S \text{ photons per pulse.}$$

Thus ordinary Raman scattering is much too weak, while resonant Raman scattering is marginal even assuming a generous enhancement. Over our assumed

100 km distance T_L and T_s will be small under most atmospheric conditions in the lower atmosphere, but they may be large in the upper atmosphere.

The second technique is based on comparing the Rayleigh (or Mie) scattered return from the region beyond the exhaust for two wavelengths, one of which is absorbed by the OH^- radical. If the two wavelengths are very close together, the attenuations due to processes other than OH^- absorption will be equal, and the difference in the return signal is due to the absorption of the outgoing beam and the return scattering.

Let us send our pulse out and not open our detector shutter until light scattered from the region beyond the exhaust is arriving. If we leave the shutter open for 5 μs, the effective scattering length is 1.5 km. (For 5 μs dye laser pulse this is the range resolution; we could use longer gate times and collect larger signals or reduce the laser pulse duration.) We observe the Rayleigh scattering from this scattering length beyond the exhaust for transmitted two wavelengths. The return signal is

$$N = \frac{E\ \kappa\ \ell\ \sigma\ \Omega\ T_L^2}{h\ \nu}$$

where the symbol are defined above. We use a wavelength of 306.63 nm for reasons given below. Then

$\kappa = 2.5 \times 10^{19}$ molecules/cm^3 assuming the scattering is from air at one atm.,

$\ell = 1.5 \times 10^{5}$ cm,

$\sigma = 6 \times 10^{-27}$ cm^2, and

$h\ \nu = 6.5 \times 10^{-19}$ J.

Then

$$N = 2.2 \times 10^{5}\ T_L^2.$$

Thus the return signal is substantially larger than for the resonant Raman scattering case. We note that the return signal will often be much larger than this value due to Mie scattering, scattering from clouds, or from the earth's surface beyond the exhaust plume.

The absorption cross section[5] of OH^- at 3000°K changes by over 10^3 in a wavelength interval a small fraction of a nm wide at 306.63 nm. At a frequency of 32,603.31 cm^{-1} the absorption cross section is 6.65 cm^{-1} atm^{-1}.

For the 1 meter diameter 1% OH^- rocket exhaust under consideration the absorption at this wavelength across the center of the exhaust is 49%. If both the outgoing beam and return scattering traversed the center the net transmission would be only 26%, while a wavelength longer by, say, 0.05 nm would be essentially completely transmitted (over 99.9%). Of course, in practice only a fraction of the outgoing beam and scattered light would cross the plume since the beam diameter would be larger than our 1 meter plume, so the signal difference between these wavelengths would be less. The signals are so large, however, that small differences could be detected.

VI. RECOMMENDATIONS FOR FURTHER WORK

Remote sensing techniques offer attractive capabilities for military intelligence applications. To achieve sensitivities and ranges of interest, clearly some resonance phenomena will be employed. Not only is high average power in a tunable laser source therefore required, but also minimum beam divergence is essential for examination of localized remote scattering volumes.

The dye Zig-Zag Face-Pumped Laser has these characteristics, and it is recommended that such a laser be developed to a more nearly optimal design. The 3x3 cm^2 aperture tested in this program is appropriate for a power amplifier stage, but a driver is required with correspondingly good optical characteristics and a power output sufficiently high to enable operation under near saturated gain conditions.

A preliminary design of such a smaller aperture device has been developed based upon data taken in this program. Design characteristics are:

- 1x3 cm^2 aperture, three pass configuration
- Same coupling configuration and hence efficiency as present module
- Three times as many dye channels in the same length module and therefore three times the gain per pass
- Input and output beam on opposite ends for experimental convenience
- Good area efficiency with a beam diameter of 0.9 cm, appropriate for an oscillator with low beam divergence

As an oscillator, based upon measurements made on the present module, and using the same pump parameters, we expect:

- Threshold, 147 J,
- Slope efficiency with a 1.0 cm diam beam, 0.5%,
- Output energy with 500 J to the flashlamps, 1.7 J,
- Point efficiency, 0.34%, and
- Average power, at 5 pps, 8.5 W.

With this output energy from the oscillator, an identical module may also be used efficiently as a three pass amplifier, where we expect:

- Net small-signal gain, 9.2 db,
- 1 J per pulse added for an input signal greater than 0.3 J,
- From 0.22%, to 0.3% efficiency as an amplifier, for inputs of 0.3 to 3 J, and
- From an oscillator-amplifier combination, up to 2.7 J output for 1000 J pump energy

Alternative configurations are feasible if, for example, a shorter pulse duration is desired.

The efficiency, high peak and average power, and low divergence of this dye laser suggest applications such as to under ocean sensing and illumination where tuning and narrow line widths are not necessarily required. For remote probing as considered elsewhere in this report, the high power dye Zig-Zag-FPL oscillator would be well suited to use in conjunction with a low power oscillator in an injection-narrowed configuration.

It is recommended therefore that a smaller aperture DZZ-FPL be designed and tested both as an oscillator and as an amplifier. Following this demonstration, a laser system of one or several modules could be assembled as deliverable hardware.

REFERENCES

1. S.D. Silverstein, Absolute Rotational Raman Cross Sections for N_2 and O_2 from the Far Infra-Red to the Ultraviolet, General Electric Corporate Research and Development Report No. 73CRD007 (December 1972).

2. R.L. St. Peters and S.D. Silverstein, A Search for Resonant Raman Scattering in ClF, Cs_2 Vapor, and Na_2 Vapor, General Electric Corporate Research and Development Report No. 73CRD042 (February 1973).

3. W.W. Morey, Injection Narrowing of a Flashlamp-Pumped Dye Laser Oscillator, General Electric Corporate Research and Development Report No. 73CRD043 (February 1973).

4. R.L. St. Peters and D.J. Taylor, The Dye Zig-Zag Face-Pumped Laser: A High Average Power, High Brightness Laser, General Electric Corporate Research and Development Report No. 73CRD059 (February 1973).

5. S.A. Golden, Spectral Absorption Coefficients of Electronic Transitions in Diatomic Molecules (U), vol. 2., part C, prepared for ARPA at North American Aviation, Rocketdyne Division, December 1965.

APPENDIX A

ABSOLUTE ROTATIONAL RAMAN CROSS SECTIONS FOR N_2 AND O_2 FROM THE FAR INFRA-RED TO THE ULTRAVIOLET

GENERAL ELECTRIC

GENERAL ELECTRIC COMPANY
CORPORATE RESEARCH AND DEVELOPMENT
Schenectady, N.Y.

ABSOLUTE ROTATIONAL RAMAN CROSS SECTIONS FOR N_2 AND O_2 FROM THE FAR INFRA-RED TO THE ULTRAVIOLET

by

S. D. Silverstein
Physics and Electrical Engineering Laboratory

Report No. 73CRD007 December 1972

TECHNICAL INFORMATION SERIES

CLASS 1

GENERAL ELECTRIC

General Electric Company
Corporate Research and Development
Schenectady, New York

TECHNICAL INFORMATION SERIES

AUTHOR	SUBJECT	NO
Silverstein, SD	Raman scattering	73CRD007
		DATE December 1972
TITLE Absolute Rotational Raman Cross Sections for N_2 and O_2 from the Far Infra-red to the Ultraviolet		GE CLASS 1
		NO. PAGES 16
ORIGINATING COMPONENT Physics and Electrical Engineering Laboratory		CORPORATE RESEARCH AND DEVELOPMENT SCHENECTADY N Y

COMPANY

An extrapolation procedure, based upon the fundamentals of light scattering theory, has been developed to predict the frequency dependence of rotational Raman cross sections for molecules not having allowed infra-red absorptions. The method incorporates the frequency dependence of the polarizability. Specific application is made to the atmospheric constituents N_2 and O_2, where the absolute rotational Raman cross sections measured at 488 nm have been used with this extrapolation procedure to obtain cross sections for the different rotational transitions at 10.6 μm, 1.06 μm, 488 nm, and 265 nm.

KEY WORDS

Raman scattering, rotation Raman scattering, nitrogen, oxygen, spectroscopy, laser sensors

INFORMATION PREPARED FOR _____

_____

Additional Hard Copies Available From

Corporate Research & Development Distribution
P.O. Box 43 Bldg. 5, Schenectady, N.Y., 12301

Microfiche Copies Available From

Technical Information Exchange
P.O. Box 43 Bldg. 5, Schenectady, N.Y., 12301

RD-54 (1070)

ABSOLUTE ROTATIONAL RAMAN CROSS SECTIONS FOR N_2 AND O_2 FROM THE FAR INFRA-RED TO THE ULTRAVIOLET*

S.D. Silverstein

I. INTRODUCTION

An accurate determination of the absolute cross-section for rotational Raman scattering from atmospheric constituents for a broad range of pump frequencies is often desired for a variety of reasons ranging from diagnostics to estimation of threshold conditions for nonlinear processes. Laboratory measurements are typically made at frequencies which optimize detection sensitivity and system stability, and these frequencies are usually in the visible. If one desires, for example, an absolute cross section in the infra-red at the CO_2 laser wavelength of 10.6μm, a direct laboratory measurement of cross sections would be very difficult since $\sigma \sim \lambda^{-4}$, and infra-red detectors do not have sensitivities comparable to detectors in the visible. In this work we develop a theoretically based extrapolation procedure to obtain rotational Raman cross sections from the infra-red to the ultraviolet for N_2 and O_2 using absolute measurements of these cross sections in the visible.

In addition to the predominant atmospheric constituents N_2 and O_2, there are also the polyatomic molecules, CO_2 and water vapor, in relatively small quantities. Both of these species have absorptions in the infra-red associated with the precence of permanent electric dipole moments for particular states of

* This research was supported by the Advanced Research Projects Agency of the Department of Defense and was monitored by ONR under Contract No. N0014-72-C-0503.

Manuscript Reveived 12/29/72

the molecules. The effect of these allowed infra-red transitions on rotational Raman scattering (RRS) in the visible is highly suppressed. They should however contribute significantly to the infra-red scattering. The conclusion we come to as far as the polyatomics are concerned, is that even with multiple determinations at different wavelengths in the visible, the contributions of the low-lying infra-red transitions cannot be determined with sufficient accuracy to develop a meaningful extrapolation from the visible to the infra-red.

II. EXTRAPOLATION PROCEDURE FOR N_2 AND O_2

The atmospheric gases O_2 and N_2 are, of course, homonuclear diatomic molecules which possess no permanent electric dipole moment. As such, the intraband dipole transitions within a given electronic manifold are forbidden, and the contributions to RRS arise solely from the effects of virtual transitions to higher lying electronic states. The transitions of interest here are those associated with rotational angular momentum changes of $\Delta N = \pm 2$.

The absolute cross sections for RRS by N_2 and O_2 at 647.1 and 488 nm have been measured.[1] We develop here a straightforward theoretically based extrapolation procedure to obtain RRS cross sections at other wavelengths using these measurements in the visible. This procedure takes into account the frequency dependence of the polarizability as well as the obvious ω^4 dependence of the Raman cross section.

Let us now develop the theoretical arguments for the extrapolation procedure. We define the states $|i\rangle$; $|f\rangle$ as the initial and final rotational states within the ground state manifold. The Raman scattering amplitude can be written as

$$\langle f|C_{\mu\nu}|i\rangle = \frac{2\pi\hbar}{V}\sqrt{\omega_{ki}\omega_{kf}}\sum_{m\alpha}\left\{\frac{(d_\mu)_{fm\alpha}(d_\nu)_{m\alpha i}}{\varepsilon_i-\varepsilon_{m\alpha}+\hbar\omega_{ki}}+\frac{(d_\nu)_{fm\alpha}(d_\mu)_{m\alpha i}}{\varepsilon_i-\varepsilon_{m\alpha}-\hbar\omega_{kf}}\right\}. \quad (1)$$

As is well known[2,3], the $C_{\mu\nu}$ form the components of a Cartesian tensor of second rank. By taking suitable linear combinations of components of this tensor we can form terms which transform in the same way as spherical harmonics of order zero, one, and two respectively. For RRS, specifically for transitions in which the rotational quantum number N changes by ±2, we are interested in the combination which transforms as the L=2 representation of the full rotation group. This form is the "symmetric form" or "quadrupole scattering"[2] defined by

$$S_{\mu\nu} = \frac{1}{2}(C_{\mu\nu} + C_{\nu\mu}) - \frac{1}{3}\delta_{\mu\nu}\sum_{\gamma} C_{\gamma\gamma} \,. \tag{2}$$

For the diagonal components we have

$$\langle f|S_{\mu\mu}|i\rangle = \frac{1}{3}\left[2\langle f|C_{\mu\mu}|i\rangle - \sum_{\gamma}(1-\delta_{\mu\gamma})\langle f|C_{\gamma\gamma}|i\rangle\right], \tag{3}$$

while for the off diagonal components we have

$$\langle f|S_{\mu\nu}|i\rangle \underset{\mu\neq\nu}{=} \frac{1}{2}\langle f|C_{\mu\nu} + C_{\nu\mu}|i\rangle \,. \tag{4}$$

From Eq. 1 we see that

$$\langle f|C_{\mu\mu}|i\rangle = -\frac{2\pi\hbar}{V}\sqrt{\omega_{kf}\omega_{ki}}\sum_{m,\alpha}(d_\mu)_{f,m\alpha}(d_\mu)_{m\alpha,i} \times\left[\frac{1}{\Delta m_\alpha - \hbar\omega_{ki}} + \frac{1}{\Delta m_\alpha + \hbar\omega_{ki} - \varrho_{fi}}\right], \tag{5}$$

where

$$\Delta m_\alpha = \varrho_{m\alpha} - \varrho_i \,.$$

Now, defining,

$$\gamma \equiv \hbar\omega_{ki}/\Delta m_\alpha \; ; \; \beta \equiv \varepsilon_{fi}/\Delta m_\alpha \; ,$$

we rewrite Eq. 5 in the form,

$$\langle f|c_{\mu\mu}|i\rangle = -\frac{2\pi\hbar}{V}\sqrt{\omega_{kf}\omega_{ki}}\sum_{m,\alpha}\left\{\frac{(d_\mu)_{f,m\alpha}(d_\mu)_{m\alpha,i}}{\Delta m_\alpha}\cdot\frac{1}{1-\gamma^2}\left[1+\beta\frac{(1-\gamma)}{1+\gamma-\beta}\right]\right\} . \qquad (6)$$

If we denote E_{10} as the band head separation between the ground vibrational-rotational state and the lowest manifold of states for which there exist allowed dipole transitions with the ground state, we have $\Delta m_\alpha > E_{10}$ for all bands, and $\beta \lesssim 10^{-3}$ for the relevant transitions in N_2 and O_2. In view of these magnitudes, we can neglect the β terms in Eq. 6. Hence, the scattering amplitude can be well approximated by

$$\langle f|c_{\mu\mu}|i\rangle \cong -\frac{2\pi\hbar}{V}\sqrt{\omega_{kf}\omega_{ki}}\sum_{m,\alpha}\frac{(d_\mu)_{f,m\alpha}(d_\mu)_{m\alpha,i}}{\Delta m_\alpha\,(1-\gamma^2)} . \qquad (7)$$

The result given here is still not in a form from which an extrapolation of a measurement at a specific frequency to other frequencies can be made. To accomplish this, we make the further approximation of replacing the γ contained within the sum of Eq. 7 by $\hbar\omega_{ki}/\Delta_{10}$; thus removing this factor from the summation.

$$\langle f|c_{\mu\mu}|i\rangle \cong -\frac{2\pi\hbar}{V}\sqrt{\omega_{kf}\omega_{ki}}\cdot\frac{1}{\left(1-(\hbar\omega_{ki}/\Delta_{10})^2\right)}\sum_{m,\alpha}\frac{(d_\mu)_{f,m\alpha}(d_\mu)_{m\alpha,i}}{\Delta m_\alpha} . \qquad (8)$$

17

Here Δ_{10} is the band head energy of the lowest electronic band exhibiting allowed dipole transitions with the ground state manifold. For O_2, Δ_{10} would correspond to the band head for the uv (Schumann-Runge bands) corresponding to the transition at an energy $\sim$ 50,000 cm^{-1}. The higher transitions that would contribute are in excess of 100,000 cm^{-1}. This, coupled with the fact that the Franck-Condon overlap integrals between the ground vibrational state and the higher continuum states are small, makes the approximation quite good. The most significant correction to the approximation will presumably occur in the variation in energy for the uv band itself. The results are, of course, appropriate only to frequencies below the band head. One can estimate the corrections to be the order of

$$\frac{4\Delta_{10}\delta(\omega^2-\omega_s^2)}{(\Delta_{10}^2-\omega^2)(\Delta_{10}^2-\omega_s^2)} \quad . \tag{9}$$

Here δ is the average band width of the excited state, ω_s is the measured frequency and ω is the extrapolated frequency. This error is the order of 5% at 10.6 μm and 15% at 300 nm with ω_s at 500 nm for O_2.

Similar conditions prevail for N_2 where the first allowed transitions are the $^1\Sigma_\mu^+ \leftarrow {}^1\Sigma_g^+$; $^1\pi_\mu \leftarrow {}^1\Sigma_g^+$ bands, both of which exhibit band head energies of $\sim$ 100,000 cm^{-1}.

The differential cross section for the "quadrupole scattering", $\Delta N = \pm 2$, is given by

$$\sigma_{\mu\nu}(\omega_{kf}) = \text{const} \frac{\omega_{kf}^3}{\omega_{ki}} \left| \langle f | S_{\mu\nu}(\omega_{ki}) | i \rangle \right|^2 . \tag{10}$$

With the approximations made, this assumes the form

$$\sigma_{\mu\nu}(\omega_{kf}) \cong \text{const}\ \omega_f^4 \left(a_0^{\mu\nu}\right)^2 \Big/ \left(1 - \left(\frac{\omega_{ki}}{\Delta_{10}}\right)^2\right)^2 , \tag{11}$$

18

where

$$a_0^{\mu\nu} \equiv \sum_{m,\alpha} \sum_{\xi,\zeta} \frac{(d_\xi)_{f,m\alpha} (d_\zeta)_{m\alpha,i}}{\Delta_{m\alpha}} \left[\frac{1}{2}(\delta_{\xi\mu}\delta_{\zeta\nu} + \delta_{\xi\nu}\delta_{\zeta\mu}) - \frac{1}{3}\delta_{\xi\zeta}\delta_{\mu\nu} \right], \tag{12}$$

as follows directly from Eq. 2.

The general result for the ratio of the rotational Raman cross section at two different frequencies is given by

$$\frac{\sigma_{\mu\nu}(\omega_{1i})}{\sigma_{\mu\nu}(\omega_{2i})} = \frac{(\omega_{1f})^4}{(\omega_{2f})^4} R(\omega_{1i}, \omega_{2i}) , \tag{13}$$

where

$$R(\omega_{1i}, \omega_{2i}) \equiv \left| \frac{1 - (\omega_{2i}/\Delta_{10})^2}{1 - (\omega_{1i}/\Delta_{10})^2} \right|^2 . \tag{14}$$

In Fig. 1, we plot $R(\omega,\omega_s)$ as a function of the ω. We have normalized the results so that ω_s corresponds to 488 nm. The deviation of $R(\omega,\omega_s)$ from unity signifies the departure of the cross section from the ω_f^4 extrapolation.

III. APPLICATION OF EXTRAPOLATION PROCEDURE

A. Determination of N_2 Rotational Raman Cross Sections

Let us now illustrate how one uses the results to compute the absolute cross sections for different rotational transitions at different frequencies and temperatures from a single absolute cross section measurement at a particular standard frequency denoted by ω_s. The ground state of N_2 is a $^1\Sigma_g^+$ state, and the total angular momentum J is just equal the rotational angular momentum N. To a good approximation, we can neglect the centrifugal distortion corrections to the rotational energy and

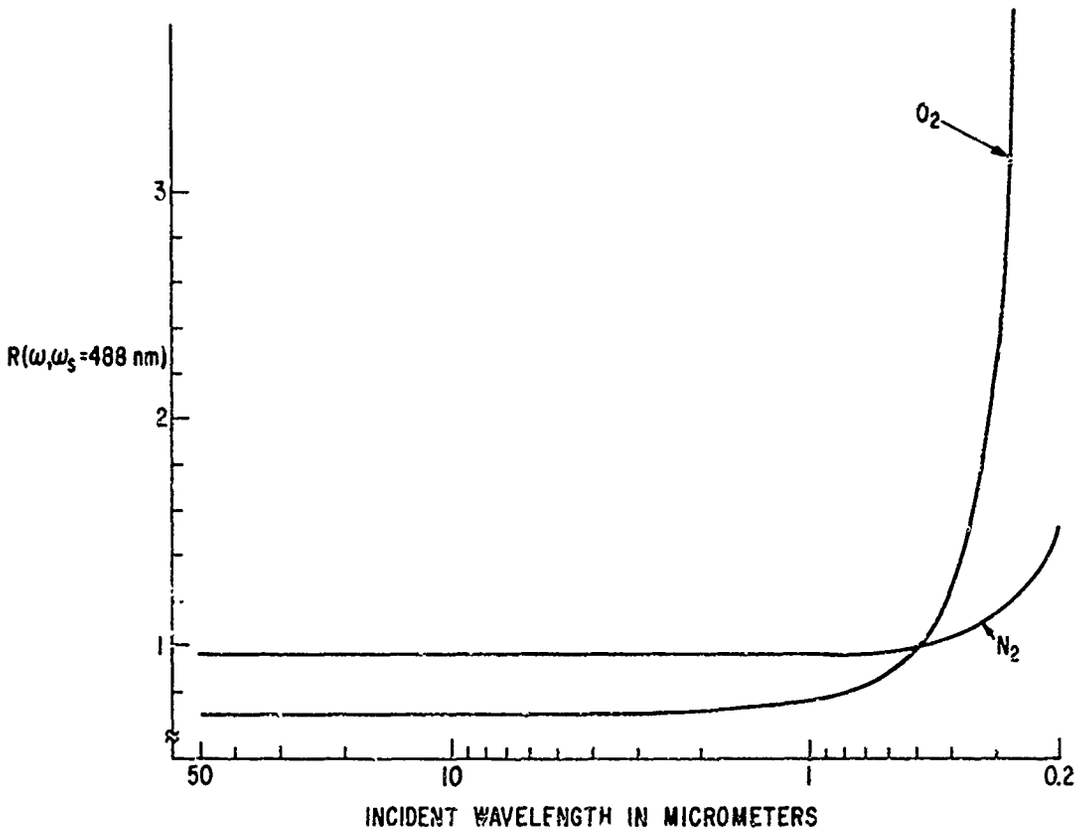

Fig. 1 A plot of the factor $R(\omega,\omega_s)$ which reflects the frequency dependence of the square of the polarizability normalized to the standard frequency, which in this case is taken at a wavelength of 488 nm.

represent the rotational energy for the vth vibrational state of the ground electronic manifold as

$$F(V,J) = B_V J(J+1) \quad . \tag{15}$$

The general expression for the differential cross section per molecule for a particular transition can be written as

$$\sigma_{\mu\nu}(V,J\pm,\omega,T) = A_{\mu\nu}(\theta)\, b_J^{J\pm2}\, P_{V,J}(T)\, \frac{\left[\omega + F(V,J) - F(V,J\pm2)\right]^4}{\left|1 - \left(\omega/\Delta_{10}\right)^2\right|^2} \quad . \tag{16}$$

Here, we have used the results of Section II for the frequency dependence. The factor $A_{\mu\nu}(\theta)$ depends upon the initial and final polarization only, and the angle θ which is defined as the angle between the incident polarization direction for plane polarized light and the final propagation direction. We have used J± to denote the transitions $\Delta J = \pm 2$ respectively. The factors $P_{V,J}(T)$ are the thermal occupation probabilities,

$$P_{V,J}(T) = \frac{g_J}{Q} \exp\left[-B_V J(J+1)/K_b T\right] \quad , \tag{17}$$

where Q is the partition function and g_J is the degeneracy factor,

$$g_J = \begin{cases} (2J+1)\, I(2I+1) & \text{for } J \text{ odd} \\ (2J+1)(I+1)(2I+1) & \text{for } J \text{ even} \end{cases} \quad . \tag{18}$$

Here I is the N nuclear spin, I = 1. The $b_J^{J\pm2}$ factors are the Placzek-Teller coefficients,

$$b_J^{J+2} = \frac{3(J+1)(J+2)}{2(2J+3)(2J+1)} \quad ; \tag{19}$$

$$b_J^{J-2} = \frac{3(J-1)J}{2(2J-1)(2J+1)} \tag{20}$$

The relation for a rotational cross section relative to a measured cross section at a frequency ω_s, temperature T_s, for the transition $J_{s\pm}$ is given by

$$\sigma_{\mu\nu}(J\pm,\omega,T) = \sigma_{\mu\nu}(J_s\pm,\omega_s,T_s)\left[\frac{\omega-\Delta\nu(J\pm)}{\omega_s-\Delta\nu(J_s\pm)}\right]^4 \frac{b_J^{J_s\pm2}}{b_{J_s}^{J_s\pm2}} \frac{g_J}{g_{J_s}} \tag{21}$$

$$\times R(\omega,\omega_s)\cdot\exp\left[\frac{Bv}{K}\left(\frac{J_s(J_s+1)}{T_s} - \frac{J(J+1)}{T}\right)\right].$$

Here

$$\Delta_v(J+) = B_v(4J+6) \; ; \quad \Delta_v(J-) = -B_v(4J-2) \cdot$$

For N_2, the value[4] of B_v is 2.010 cm^{-1}. Absolute cross sections for O_2 and N_2 have recently been obtained[1] at 488.0 nm, T_s = 296°K. These are giv- by

$$\sigma_{11}(6+, 20,492\ cm^{-1}, 296°K) = (5.963 \pm 0.60)\times10^{-31}\ cm^2/sr\ ;\ N_2 \tag{22}$$

$$\sigma_{11}(9+, 20,492\ cm^{-1}, 296°K) = (1.936 \pm 0.20)\times10^{-30}\ cm^2/sr\ ;\ O_2 \tag{23}$$

These are the differential cross section for 90° scattering, the results are the same in the forward direction. We can use the standard depolarization ratios of 3/4 to obtain the cross section for the emission polarization perpendicular to the incident.

In Table I, we have tabulated the cross sections at different frequencies corresponding to the wavelengths 10.6 μm (CO_2 laser), 1.06 μm (neodymium lasers), 488 nm (argon ion standard), and 265 nm (quadrupled Nd) from the measured absolute value at 488 nm (Eq. 22) using the relation of Eq. 21. Any other desired wavelengths can be computed using this relation.

B. Determination of O_2 Rotational Raman Cross Sections

Detailed analyses of the relative intensities of RRS at a fixed pump frequency have been made[5-7], and the reader is referred to these works for details.

The case of O_2 is conceptually a more difficult application than N_2. This is due to the fact that the ground state of oxygen is a spin triplet, $^3\Sigma_g^-$, and the coupling between the rotational angular momentum $\underset{\sim}{N}$ and the spin $\underset{\sim}{S}$ splits the spin degeneracy into three states of total angular momentum N+1, N, N-1. For the temperatures of interest, the splittings are small compared to K_bT and one can simply use the same exponential factor for the thermal occupancy of each member of the triplet. The differences in occupancy among the triplet can be taken simply as the difference in their degeneracy factors. The nuclear spin of oxygen is zero, hence to preserve the symmetry of the molecular wave function upon inversion, only odd integral values of the rotational quantum numbers N are allowed. The possible rotational Raman transitions which occur are given by the selection rules $\Delta N = 0, \pm 2$, and $\Delta J = 0, \pm 1, \pm 2$.

In Fig. 2, we have illustrated the set of allowed Stokes and anti-Stokes transitions starting from the central triplet with rotational quantum number N. We have used the standard spectroscopic notation to label these transitions, viz $^{(\Delta N)}_{\Delta J}$, where

TABLE I ABSOLUTE DIFFERENTIAL CROSS SECTIONS FOR

N_2 AT 0°C IN cm^2/sr*

ROTATIONAL STATE N	% POP AT 0°C	TRANSITION N-N'	10.6 μm $x10^{-37}$	1.06 μm $x10^{-33}$	488 nm $x10^{-31}$	265 nm $x10^{-30}$
0	1.4	0-2	6.36	6.78	1.62	2.33
1	2.1	1-3	5.41	5.95	1.43	2.05
2	6.6	2-0	6.61	6.43	1.53	2.19
		2-4	14.3	16.2	3.90	5.61
3	4.4	3-1	5.77	5.45	1.29	1.85
		3-5	8.40	9.85	2.37	3.41
4	10.3	4-2	15.7	14.35	3.40	4.86
		4-6	18.3	22.13	5.33	7.67
5	5.7	5-3	9.44	6.39	1.98	2.84
		5-7	9.40	11.8	2.83	4.09
6	11.8	6-4	21.1	18.2	4.29	6.14
		6-8	18.4	23.8	5.76	8.31
7	5.9	7-5	11.1	9.32	2.20	3.14
		7-9	8.70	11.6	2.82	4.06
8	11.2	8-6	22.4	18.3	4.29	6.12
		8-10	15.8	21.9	5.30	7.66
9	5.2	9-7	10.3	8.58	2.01	2.87
		9-11	6.96	9.95	2.42	3.49
10	9.2	10-8	20.2	15.6	3.65	5.20
		10-12	12.9	17.6	4.28	6.19
11	4.0	11-9	9.15	6.85	1.60	2.28
		11-13	4.93	7.54	1.84	2.66
12	6.8	12-10	16.0	11.7	2.72	3.88
		12-14	7.95	12.6	3.08	4.46
13	2.8	13-11	6.82	4.83	1.13	1.60
		13-15	3.12	5.12	1.25	1.82
14	4.4	14-12	12.3	7.79	1.81	2.57
		14-16	4.76	8.10	1.99	2.88
15	1.7	15-13	4.55	3.05	0.709	1.01
		15-17	1.77	3.13	0.768	1.12
16	2.6	16-14	7.15	4.67	1.08	1.53
		16-18	2.58	4.71	1.16	1.68

* The results given here are the differential cross sections for incident and emitted radiation plane polarized in the same direction with the emission wave vector at 90° to the incident polarization. To obtain the depolarized component at 90°, the results are to be multiplied by 3/4.

We note that the cross sections given here have incorporated the thermal occupation factors of the rotational levels. To eliminate this population factor one merely divides by the relative population for each rotational state as given in the table.

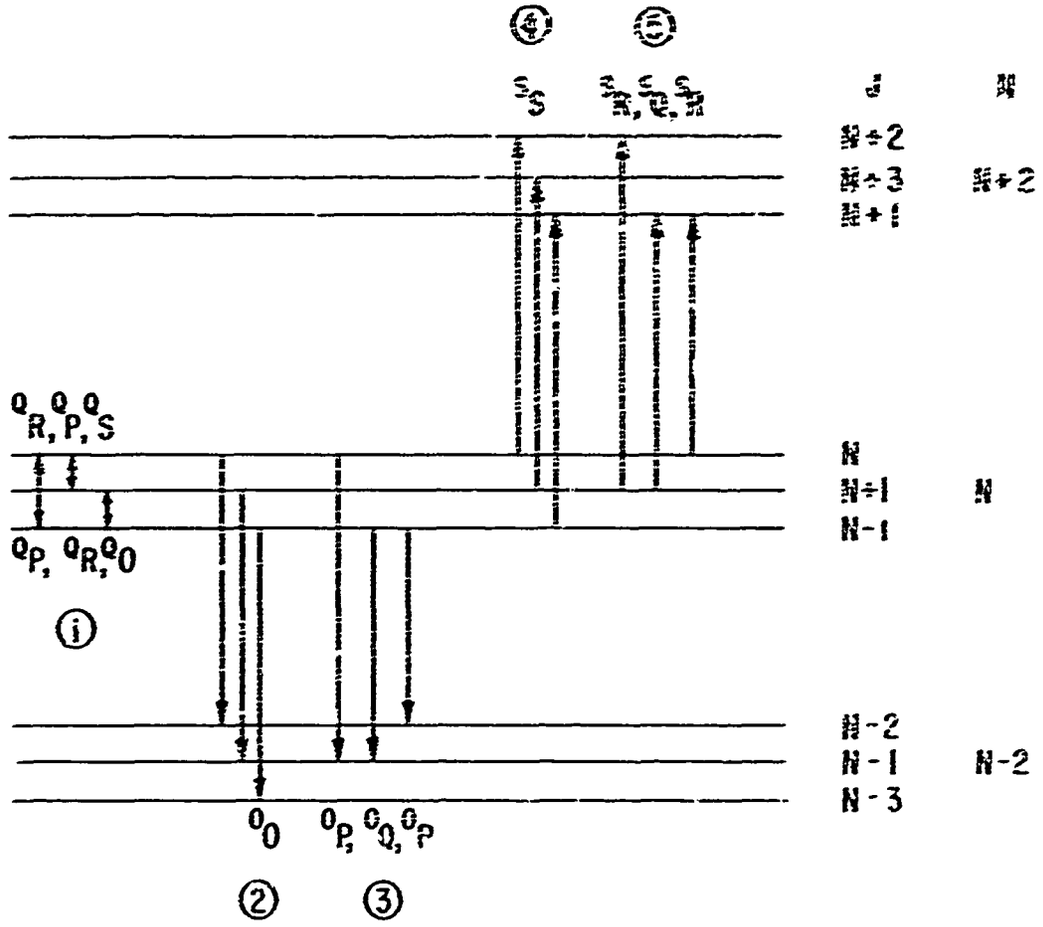

Fig. 2 An illustration of the allowed rotational Raman branches in O_2. The group designated by (1) appear as satellite lines on the Rayleigh scattering, while (2), (3) are anti-Stokes, and (4), (5) are the Stokes scattering.

the branches (O, P, Q, R, S) correspond to the angular momentum changes (-2, -1, 0, +1, +2) respectively. The group of transitions designated by (1) in Fig. 2 corresponds to the transitions $\Delta N = 0$, and will appear as satellites on the Rayleigh line. There are, of course, no satellites of this kind on the N_2 Rayleigh line. We see that the triplet nature splits the $\Delta N = \pm 2$ Stokes and anti-Stokes transitions into six separate transitions, each of which has a different intensity factor. The intensity factors are given by the coefficients[5-7] $b_{JN}^{J''N''}$ where for the three ^{S}S components we have,

$$b_{N+1,N}^{N+3,N+2} = \frac{3(N+1)(N+2)(2N+7)}{2(2N+1)(2N+5)} ; \qquad (24)$$

$$b_{N-1,N}^{N+1,N+2} = \frac{3(2N-1)(N+3)(N+1)}{2(2N+3)(2N+1)} ; \qquad (25)$$

$$b_{N,N}^{N+3,N+2} = \frac{3N(N+3)}{2(2N+3)} ; \qquad (26)$$

while for the two ^{S}R components,

$$b_{N,N}^{N+1,N+2} = \frac{3}{2N+3} \qquad (27)$$

$$b_{N+1,N}^{N+2,N+2} = \frac{3}{2N+3} \qquad (28)$$

and finally for the ^{S}Q component,

$$b_{N+2,N}^{N+2} = \frac{9}{(2N+1)(2N+3)(2N+5)} \quad (29)$$

The sum of these coefficients satisfies the general relation,

$$(2N+1)\,b_N^{N-2} \equiv \frac{1}{(2N+1)} \sum_{J,J'} b_{J,N}^{J',N+2} \quad (30)$$

where the b_N^{N-2} are the Placzek-Teller coefficients as given in Eqs. 19, 20. This general result can be derived mathematically from the symmetry relations on the 3-j and 6-j coefficient[3] of which the general form of $b_{J,N}^{J',N'}$ can be expressed[5].

Alternatively, the results are obvious on the basis of physical grounds as the relative intensities are independent of the spin-rotational coupling. Hence, the total intensity must be the same as if the splitting were zero, where the only difference between the Placzek-Teller coefficients as given for N_2 are the spin degeneracy factors. For O_2, the levels are spread over a broader channel which is the order of the triplet splitting. On the Stokes side, the channel width will be maximum for N equal to 1, where the three ^{S}S components form a central channel with the two ^{S}R components forming smaller side bands at a separation $\sim 2\ cm^{-1}$ from the central channel. At higher N, the ^{S}S components dominate. and the central channel width is narrower. Similar results are obtained for the anti-Stokes.

In Table II we have computed the absolute differential cross section associated with possible transitions for $\Delta N = \pm 2$. We have summed all the J values associated with the initial and final N's. The expressions used for the computations here are identical in form to that used for the N_2 computation in Eq. 16, except of course, that we have modified the various terms and parameters as discussed in this section to make them appropriate to O_2.

TABLE II ABSOLUTE DIFFERENTIAL CROSS SECTIONS FOR

O_2 AT 3°C IN cm^2/sr*

ROTATIONAL STATE N	% POP AT 3°C	TRANSITION N-N'	10.6 μm $x10^{-36}$	1.06 μm $x10^{-32}$	488 nm $x10^{-30}$	265 nm $x10^{-29}$
1	4.4	1-3	2.43	2.77	0.830	3.57
3	9.6	3-1	2.55	2.59	0.773	3.32
		3-5	3.97	4.72	1.42	6.12
5	13.1	5-3	4.32	4.21	1.25	5.37
		5-7	4.79	5.96	1.80	7.75
7	14.7	7-5	5.40	5.04	1.50	6.41
		7-9	4.89	6.37	1.93	8.32
9	14.4	9-7	5.73	5.13	1.52	6.49
		9-11	4.43	6.05	1.84	7.93
11	12.6	11-9	5.39	4.63	1.36	5.83
		11-13	3.63	5.21	1.58	6.85
13	10.1	13-11	4.59	3.78	1.11	4.75
		13-15	2.73	4.11	1.25	5.42
15	7.5	15-13	3.58	2.83	0.832	3.55
		15-17	1.85	2.99	0.914	3.96
17	5.1	17-15	2.58	1.96	0.574	2.44
		17-19	1.21	2.02	0.618	2.68
19	3.2	19-17	1.72	1.26	0.367	1.56
		19-21	0.724	1.27	0.389	1.68
21	1.9	21-19	1.06	0.749	0.218	0.927
		21-23	0.402	0.740	0.228	0.991

* The results given here are the differential cross sections for incident and emitted radiation plane polarized in the same direction with the emission wave vector at 90° to the incident polarization. To obtain the depolarized component at 90°, the results are to be multiplied by 3/4.

We note that the cross sections given here have incorporated the thermal occupation factors of the rotational levels. To eliminate this population factor one merely divides by the relative population for each rotational state as given in the table.

28

ACKNOWLEDGMENTS

The author would like to thank Drs. M. Lapp, C.M. Penney and D.R. White for valuable discussions.

The measurements of absolute rotational cross sections in the visible which have been used in this study and reported in Ref. 1 were obtained in a program supported by Lewis Research Center of NASA under contract NAS3-15825 with technical direction by J.A. Salzman.

REFERENCES

1. C.M. Penney, M. Lapp, and R.L. St. Peters, "Rotational Raman Scattering Cross Sections for N_2, O_2, and CO_2", General Electric Corporate Research and Development Report (to be issued), Schenectady, New York (1972).

2. G. Placzek, Handbuch der Radiologie, Edited by Erich Marx, Liepzig, Academische Verlagsgesllschaft, VI, 2, (1934).

3. See for example, A.R. Edmonds, "Angular Momentum in Quantum Mechanics", 2nd ed. Princeton University Press, Princeton (1960).

4. G. Herzberg, "Spectra of Diatomic Molecules", 2nd Edition, D. Van Nostrand Company, Inc., New York (1950).

5. D.L. Tenschler, J.L. Hunt, T.K. McCubbin and S.R. Polo, J. Mol. Spectry 31, 173 (1969).

6. D.W. Lepard, Canadian Journal of Physics 48, 1664 (1970).

7. K. Altmann, G. Strey, J.G. Hochenbleicher and J. Brandmüller, Z. Naturforsch 27, 56 (1972).

29

APPENDIX B

A SEARCH FOR RESONANT RAMAN SCATTERING IN ClF, Cs_2 VAPOR, AND Na_2 VAPOR

GENERAL ELECTRIC

GENERAL ELECTRIC COMPANY
CORPORATE RESEARCH AND DEVELOPMENT
Schenectady, N.Y.

A SEARCH FOR RESONANT RAMAN SCATTERING IN ClF, Cs_2 VAPOR, AND Na_2 VAPOR

by

R. L. St. Peters and S. D. Silverstein
Physics and Electrical Engineering Laboratory

Report Number 73CRD042 January 1973

TECHNICAL INFORMATION SERIES

CLASS 1

ENERAL ELECTRIC

eneral Electric Company
orporate Research and Development
chenectady, New York

TECHNICAL INFORMATION SERIES

AUTHOR	SUBJE	NO
St. Peters, RL Silverstein, SD	Raman	73CRD042
		DATE January 1973
TITLE A Search for Resonant Raman Scattering in ClF, Cs_2 Vapor, and Na_2 Vapor		GE CLASS 1
		NO PAGES 14
ORIGINATING COMPONENT Physics and Electrical Engineering Laboratory		CORPORATE RESEARCH AND DEVELOPMENT SCHENECTADY, N Y.

SUMMARY

The re-emission spectra of three gases upon excitation by radiation from slightly tunable ion lasers were examined for evidence of resonant enhancement of Raman scattering. The absorption of ClF was found to be too weak to cause observable resonance enhancement, and the absorption spectrum of Cs_2 is too complex to isolate resonance effects of a single line. Using a single-mode argon ion laser to excite the $6 \leftarrow 0$ P(28) Na_2 absorption line at 476.5 nm, a re-emission was observed under sufficiently-far-from-resonance conditions to suggest that the re-emission is resonant Raman scattering. Due to the difficult nature of the necessary experiments on Na_2 vapor, we were unable to demonstrate that this re-emission had the properties expected of resonant Raman scattering. The enhancement over ordinary Raman scattering from nitrogen gas was found to be about 10^7.

KEY WORDS

Raman, Na_2, Cs_2, ClF, resonance

INFORMATION PREPARED FOR _____

Additional Hard Copies Available From

Corporate Research & Development Distribution
P.O. Box 43 Bldg. 5, Schenectady, N.Y., 12301

Microfiche Copies Available From

Technical Information Exchange
P.O. Box 43 Bldg. 5, Schenectady, N.Y., 12301

A SEARCH FOR RESONANT RAMAN SCATTERING IN ClF, Cs_2 VAPOR, AND Na_2 VAPOR*

R.L. St. Peters and S.D. Silverstein

I. INTRODUCTION

Raman scattering from gases occurs at one or more wavelengths which are shifted in energy from the incident wavelength by vibrational-rotational energy level spacings of the molecules. Different gases thus scatter at different wavelengths, and this, plus the fact that the scattering is proportional to the partial pressure of the scattering species, make Raman scattering an attractive phenomenon for use in gas analysis. Furthermore, Raman scattering also contains temperature information.

Unfortunately, Raman scattering is a weak process. However, Raman scattering can in principle be enhanced by using an incident wavelength near an absorbing region of the scattering species. While enhancement of Raman scattering due to continuum absorption has been observed, the largest potential enhancements are for the case of an excitation wavelength near an individual isolated absorption line. Such an example has not been demonstrated. One example in I_2 vapor was reported[1] but has been found to be incorrect.[2]

The problem is a technological one due to the stiff requirements on the laser bandwidth, stability, and tunability. The bandwidth requirement comes from the importance of not having any incident radiation fall within the absorption line, since the resulting absorption causes fluorescence at the same wavelengths as the Raman scattering. Although this fluorescence is stronger than the Raman scattering, its intensity has the undesirable feature of being dependent on the partial pressures of other species in the scattering region. The long life of the intermediate state in fluorescence allows collisions with foreign gas molecules to de-excite the scattering species molecules, reducing the fluorescence. The long intermediate state lifetime also prevents accurate ranging.

The stability and tunability requirements come from the sharp dependence of the enhancement on the incident wavelength. Adequate tunable dye lasers are just now on the fringe of the state-of-the-art, and the spectral coincidences necessary to demonstrate the phenomenon with other slightly tunable

* This research was supported by the Advanced Research Projects Agency of the Department of Defense and was monitored by ONR under Contract No. N00014-72-C-0503.

Manuscript Received 1/30/73

lasers limit the selection of gases to a few, each with its own peculiar problems. Experience gained in investigating these molecules has shown that demonstrating the Raman-like character of the return signal is perhaps more difficult than finding that signal.

II. APPARATUS

The light sources used for the experiments are two Coherent Radiation model 52B ion lasers, one with an argon tube and the other a krypton tube. A prism is used as the high reflectivity cavity mirror to obtain lasing on a single spectral line. A tilted Coherent Radiation stabilized etalon is used in the laser cavity to force the oscillation to occur on a single longitudinal mode of the cavity. Tilting the etalon tunes the wavelength over the gain bandwidth of the chosen spectral line. For the strongest line at 514.5 nm the Ar ion laser yields more than 0.5 W single mode, stable to $\sim 10^{-4}$ nm over several hours, and tunable over an interval of about 0.01 nm. On the weaker lines the power is less and the tuning range is smaller.

Scattered light is collected by a lens and spectrally filtered by a Spex 1400 double monochromator using 500 nm blaze gratings with 1200 lines per mm. With narrow slit settings this instrument is capable of resolution near 0.01 nm.

The light is detected by an RCA C31000E photomultiplier which is cooled to about -40°C. Photoelectron counting techniques are used to reduce the photomultiplier dark signal.

The scattering cells are pyrex cylinders 2.5 cm long and 5 cm in diameter with a pyrex window fused to each end. The scattered light is viewed through one of these windows. The laser beam passes through the cell via the cylindrical wall perpendicular to the viewing axis. A hollow pyrex tube is attached to the cell at one point on the cylindrical wall. In the case of the cells used for the ClF work this tube led to a valve connecting the cell to a gas handling system. For the alkali metal vapor work this tube was sealed off about 10 cm from the cell and contained the alkali metal reservoir. An oven was made for the cells for the alkali metal experiments by placing the cell in a brass cylinder about 20 cm long with the cylinder axes of the cell and brass tube colinear and the cell stem projecting out of a hole in the brass tube wall. Heating tape and insulation were wrapped around the brass cylinder, and the ends were closed by glass windows. The laser beam passed through two holes in the oven wall. A copper tube was placed over the cell stem and a nichrome wire heater plus insulation were wrapped around this extension. Two thermocouples separately monitor the temperature near the end of the extension and at a point on the cell wall. To prevent metal

condensation on the cell walls the cell was kept 10°C warmer than the stem. The temperatures used for most of the Na_2 work were 285°C at the cell and 275°C at the stem end, although the cells have been heated as hot as 425°C. At 425°C the cell turns brown in about 15 minutes due to reaction of the sodium and pyrex. At 285°C a cell can be used for several days, gradually darkening. Below about 250°C there is very little Na_2 fluorescence due to the vapor pressure being too low.

This arrangement using sealed off cells makes experiments on foreign gas effects difficult. A new cell must be constructed for each foreign gas pressure, and the oven must be partially dissembled and re-assembled to change the cell. Absolute intensity comparisons from cell to cell are difficult to make with accuracy, since there is always an uncertainty in the exact temperature of the cell, and the vapor pressure is a strong function of temperature. Further, the intensity from any one cell at constant temperature is not constant but decreases due to darkening of the cell walls. Thus accurate quenching experiments would require a much more elaborate cell and are beyond the scope of this investigation. As discussed below such experiments must be done with great care.

The apparatus used in these experiments has been carefully calibrated for use in absolute Raman scattering cross section measurements.[3] The calibration has remained constant over more than a year.

III. CHLORINE FLUORIDE EXPERIMENTS

A. Introduction

Chlorine fluoride, ClF, was selected as a candidate for resonance experiments because its tabulated absorption spectrum in the visible matches the region over which a number of Kr and Ar ion laser wavelengths are available. Unfortunately, these absorption bands are extremely weak, and we found no indications of absorption or fluorescence. Ordinary Raman scattering was observed and its wavelength dependence was measured to be $(1/\lambda_R)^4$, indicating the absence of any resonance effects.

The absorption spectrum of ClF was reported by Wahrhaftig[4] in 1942. This short letter reports molecular constants and band heads, but does not give any indication of the strength of the absorption. Other band origins are listed in Pearse and Gaydon[5]. The reported absorption consists of a series of bands from 455 nm to 523 nm, plus a continuum beyond the dissociation limit at 465 nm. Six important Ar and Kr ion laser lines exist in the interval covered by the band absorption, one Ar ion line at 457.9 nm is in the continuum, and several Kr laser lines are to the red of the absorption region. Thus measurements of the Raman scattering cross sections at a number of these wavelengths would be expected to show deviations from the $(1/\lambda_R)^4$ wavelength dependence. Furthermore, three laser lines at 476.2, 476.5, and 496.5 nm lie within bands near the band origin. Calculations using the molecular constants from Herzberg[6] indicated a density of absorption lines near 476.2 nm of about 50 lines per nm. Thus it was likely that one or more ClF absorption lines would be within the gain bandwidth of an ion laser operating on one of the three lines near band origins. This would afford the opportunity of tuning a single-moded ion laser near a single absorption line to examine the re-emission for resonance enhancement of Raman scattering.

B. Experimental Results

The cell was initially filled with about 1 torr of ClF gas and the laser beam was passed through the cell. All the available Ar and Kr ion laser wavelengths were tried, one at a time, while the cell was visually observed for signs of fluorescence. None was seen. This was repeated at several pressures up to 240 torr with still no sign of any fluorescence. Since the gas in the cell was still completely clear and untinted at 240 torr it was apparent that the listed absorption in the visible must be very weak.

37

At the 240 torr pressure the Raman scattering from the Cl^{35} was measured using the spectrometer system and five different Ar ion laser wavelengths. The system used for these measurements has been carefully calibrated for Raman scattering cross section measurements. Both its relative and absolute spectral responses have been monitored for over a year and found not to vary significantly. The measured intensities of the Raman scattering from ClF at the five wavelengths were corrected for this known system response and for the incident power. Each intensity was then multiplied by the appropriate $(\lambda_R)^4$. The resultant normalized intensities should all be the same if no resonant effects are occurring, while resonance effects should cause substantial changes with incident wavelength.

The results are shown in Table I. The intensities shown have been multiplied by $(\lambda_R)^4$ and are normalized to the intensity obtained using the 514.5 nm incident wavelength. Within experimental error they are all equal, indicating the absence of resonance effects. The last entry in Table I was obtained using a Kr ion laser wavelength on a different day using a different ClF sample.

λ_{IN}, nm	$I_{RAM} \times \lambda_R^4$
457.9	1.02
476.5	0.92
488.0	0.99
496.5	1.06
514.5	1.00
530.8	0.96

TABLE I

Raman scattered intensity for six incident wavelengths. The intensities have been multiplied by λ_R^4 to eliminate the $(1/\lambda_R)^4$ dependence and are normalized to the intensity at 514.5 nm.

IV. ALKALI METAL VAPOR EXPERIMENTS

A. Introduction

A fraction of alkali metal vapors consists of diatomic molecules which absorb in the visible and emit resonance fluorescence. These molecules, including cross-alkali molecules, have long been studied via their absorption and by resonance fluorescence.[6] Although the molecular fraction of the vapor is known to increase rapidly with temperature, the actual values of the fractions are subject to some disagreement.[7,8]

A review of the absorption spectra and vapor pressures indicated Cs_2 and Na_2 were the most likely candidates for resonance studies. Both Cs_2 and Na_2 have absorption maxima in the blue where Ar ion lasers yield a number of lines. Cs_2 has a higher total vapor pressure but a smaller molecular fraction and lower oscillator strengths. We therefore chose Cs_2 for the first experiment in the hope that its higher vapor pressure would allow work at lower temperatures. However, initial experiments eliminated Cs_2 on the basis of the complexity of its spectra, and subsequent experiments focussed on Na_2.

A re-emission intensity which can be identified as resulting from resonance with the 6 ← 0 P(28) absorption line has been observed with the laser sufficiently far from this line that the re-emission is expected to be resonant Raman scattering, but we were unable to demonstrate its Raman-like character.

B. Cs_2 Experiments

Cs_2 was found to emit readily visible fluorescence when an Ar ion laser at 488.0 nm was used as the excitation source. Weaker fluorescence was observed using other laser lines. It was found, however, that even at 488 nm a temperature of over 300°C was necessary to obtain a strong signal, probably due to a combination of the low oscillator strengths and small molecular fraction. The Cs_2 re-emission showed little intensity change as the single-mode Ar laser was tuned over the gain bandwidth of several laser lines. The lines of the Cs_2 absorption spectrum are thus extremely finely spaced. Furthermore, the total pressure of Cs_2 at 300°C is over 2 torr and the individual absorption lines may be broadened by collisions leading to overlap. Thus the absorption spectrum of Cs_2 appears to be effectively a continuum not suitable for our resonance experiments.

C. Na_2 Experiments

Sodium vapor yields visible fluorescence when excited with several Ar ion laser lines. The fluorescence can be observed as a yellow-green line where

the beam passes through the cell. The strongest fluorescence is excited by the 476.5 nm line. Usable fluorescence is also obtained using the 488.0 nm line. The fluorescence obtained using other lines is much weaker. Most of our attention was given to the 476.5 nm line.

We have observed fluorescence generated by absorption at five individual rotational-vibrational lines of Na_2 which fall within the tuning range of our single mode Ar ion laser at 476.5 nm. These lines are identified in Table II along with their calculated wavelengths and their approximate position within the tuning range. We identified these lines by use of calculated wavelengths using molecular constants from Ref. 6 and by observation of the fluorescence spectra resulting from exciting each of these lines. Saturation techniques have shown that any hyperfine structure of the (10 ← 3) P(13) is negligible compared to the 24 MHz natural line width,[9] and we do not expect hyperfine structure to be significant for any of the other lines.

If the incident wavelength lies on a single isolated absorption line, say the 6 ← 0 P(28) line, a single rotational-vibrational-electronic state is being excited, in this case the J = 27 v = 6 sublevel of the $B\ ^1\pi_u$ electronic level.

Transition	Calculated λ, nm	Observed Position under 476.5 nm Gain Curve
6 ← 0 P(28)	476.479	Near red end
10 ← 3 P(13)	476.470	Slight blue of center
11 ← 3 R(59)	476.485	Near blue end
19 ← 9 P(1)	476.514	Near center
19 ← 9 R(7)	476.513	Near red end

TABLE II

Transitions identified within the Ar-ion 476.5 nm laser bandwidth. All transitions involve a change in electronic state $B\ ^1\pi_u \leftarrow X\ ^1\Sigma_g^+$. The calculated wavelengths use the molecular constants in reference 6 and are wavelengths in air. The constants are less accurate for transitions between higher vibrational states. The last transition may also be the 19 ← 9 R(6) line with a calculated λ of 476.511 nm.

Fluorescence transitions can occur from this level to lower levels where allowed by selection rules. We restrict our attention to transitions back to the $X\ ^1\Sigma_g^+$ ground electronic state. The only selection rule is then $\Delta J = \pm 1$. There will be two transitions to each vibrational sublevel of the ground state. For example, the pair 6 → 1 P(28) and R(26) are the only allowed transitions to

the v = 1 level of the ground state. Thus each vibrational fluorescence "band" consists of a doublet. The vibrational separation for Na_2 is about 2.5 nm and the doublet separation, which depends on J, for this case is about 0.4 nm.

We note that if the fluorescence occurs on the 6 - 1 P(28) line the net change in the quantum state of the molecule after absorption and re-emission is $\Delta v = +1$, $\Delta J = 0$. The 6 - 1 R(26) fluorescence line results in a net change $\Delta v = +1$, $\Delta J = -2$. Thus this fluorescence re-emission is analogous to two lines of ordinary Raman scattering, one in the Q-branch (the so-called "vibrational line") and the other in the O-branch (or the "rotational wing"). From this observation two points are clear: 1) proximity of the incident wavelength to the 6 - 0 P(28) line can only cause enhancement of two of the many rotational lines of the stokes fundamental, and 2) the resonance effects of the various absorption lines under the 476.5 nm gain curve can be separated by observing the spectrum of the re-emission. We note also that only scattering from molecules which are in the v = 0 J = 28 state can be enhanced by proximity to the 6 - 0 P(28) line.

When the incident wavelength is centered on this absorption line, the first stokes fluorescence spectrum consists of the resulting fluorescence doublet plus a weaker doublet du to the 19 - 9 P(6) line. The lines of this latter doublet are closer together than the first doublet and lie between the lines of the first doublet. We note that the v = 9 level of the ground electronic state is some 1575 cm^{-1} above the v = 0 level and is expected to be only slightly populated at 300°C where kT is only ~ 400 cm^{-1}.

This absorption line appeared particularly promising as a candidate for resonant Raman scattering experiments. It lies near the red edge of the gain curve, allowing tuning the laser from the center to more than 5 GHz (~ 0.0045 nm, or nearly the full gain curve width) off center. The resulting re-emission doublet can still be clearly identified and separated from other fluorescence lines when the laser is tuned 4.0 GHz from the center, although fluorescence caused by absorption lines near the blue edge of the gain curve interferes with this doublet further out.

The width of this line is determined essentially by its natural linewidth. The natural linewidth of the 10 - 3 P(13) transition has been measured by saturation techniques[9] and found to be ~ 24 MHz. The width of the 6 - 0 P(28) transition we are interested in is unlikely to be much different. No hyperfine structure was found in Ref 9. The total sodium pressure, atoms plus molecules, is about 10^{-2} T at 300°C. Under these conditions a molecule will pass within 1 nm of another molecule or atom about once every 1.5 μs. This

is about 225 times the lifetime of the upper level, so line broadening due to quenching of the upper level is unlikely. Since the molecule can travel 1 cm in about 2×10^{-12} sec, the molecules spend about 10^{-5} of the time within 1 cm of another atom or molecule. Thus, unless longer range forces are important, perturbations of the energy level by collisions should not be important. Longer range Van der Waals forces do exist, but they are unlikely to be able to cause significant changes in the absorption line tails.

The only remaining source of broadening is doppler broadening. For our purposes it is most convenient to treat the doppler broadening as a broadening of the incident laser line. We thus consider a laser spectrum which has a gaussian spectral profile of width 1.5 GHz[9] incident on molecules whose absorption profile is lorentzian with a 24 MHz natural linewidth.

When the laser is 4 GHz from the absorption line center, we are 166 linewidths away from resonance. Since the gaussian doppler profile of the laser is down by 4×10^{-13} at the absorption line center, we can consider the laser radiation as effectively contained within its gaussian width of 1.5 GHz. The laser is then spread over the region from 3.25 to 4.75 GHz away from resonance, i.e., from 135 to 200 linewidths from resonance. This is far enough removed that we expect the observed return re-emission signal to be Raman-like, i.e., to be resonant Raman scattering.

Several experiments can, in principle, test whether the signal is resonant Raman scattering rather than fluorescence. The important distinguishing property is that Raman scattering is independent of foreign gas pressure, i.e. it does not quench. While simple in principle, considerable care is necessary in interpreting experiments based on this test. If our excitation wavelength is in the tail of the absorption line, but close enough so that the re-emission is fluorescence, introduction of a foreign gas can still lead to little change in the re-emission over certain pressure ranges. Foreign gas pressure can, in fact, cause an increase in fluorescence[10]. To see this, we note that a foreign gas has two effects. The first is to collisionally de-excite some of the molecules, which quenches or reduces the fluorescence. The second is to broaden the absorption line. This broadening causes more absorption in the tails where our excitation wavelength is. More absorption means more excitation which will tend to increase the fluorescence. Under appropriate conditions this latter effect dominates and the fluorescence rises. Introduction of more foreign gas will eventually broaden the line sufficiently to encompass our excitation wavelength within the increased linewidth. Further

broadening will reduce the absorption, and thus the fluorescence intensity will decrease. Thus foreign gas pressure dependence experiments require careful measurements of the re-emission intensity at a number of foreign gas pressures. For experimental reasons (see Section II) such experiments are very difficult in Na_2.

Foreign gas molecules can cause collisional transfer of excitation energy to other excited states from the optically pumped ones, causing the appearance of fluorescence from these other excited states. The presence of radiation from states which are populated by collisional transfer from the optically pumped state is in itself evidence that the re-emission is fluorescence rather than Raman scattering. If the intermediate state lifetime is too short to allow collisional quenching, it is too short for collisional transfer. Such fluorescence from nearby rotational states populated by collisional transfer forms a readily visible array of fluorescence lines in each vibrational fluorescence band in fluorescence spectra from I_2 vapor[11]. This fluorescence is induced by I_2-I_2 collisions in the absence of any foreign gas and increases in intensity very rapidly with low pressures of a foreign gas.

Such fluorescence is, however, not visible in pure Na_2 even when the laser is centered on a resonance and the signal is thus known to be fluorescence. This is probably due to the short lifetime and low collision frequency. We constructed several Na_2 scattering cells with various pressures of Ar gas in an attempt to cause collisional transfer and generate this fluorescence. Only very faint traces of fluorescence from states populated by collisional transfer was found. This fluorescence would be too weak to see when exciting the resonance in its tails even if it maintained a constant ratio to the main fluorescence from the optically pumped states. Argon pressures up to 50T were used; at this pressure the fluorescence was severely quenched on the resonance center. We are unable to state an accurate quenching figure due to difficulty in comparing intensities from cell to cell, and can only say that the quenching on resonance center was at least a factor of 10. The quenching with excitation in the tails appeared less but we cannot say that none occurred. The factor of 10 quenching on line center indicates that collisions are clearly the dominant de-excitation process; the absence of fluorescence from states populated by collisional transfer indicates that the favored collision result is to de-excite the molecule rather than transfer its energy to another nearby excited state.

When compared to ordinary Raman scattering from nitrogen gas, the re-emission we observed in Na_2 is enhanced by about 10^7. This figure was obtained using the value for the Na_2 molecular fraction from Ref. 8. In view of this large enhancement, it would be indeed interesting to determine whether this re-emission is resonant Raman scattering. The necessary quenching experiments are possible but are beyond the scope of this investigation.

VI. CONCLUSIONS

The visible transition rates of ClF gas are too small to cause observable enhancement of Raman scattering. The enhancement is proportional to the product of two of these transition probabilities.

The absorption spectrum of Cs_2 molecules consists of lines which are too closely spaced to permit isolation of resonance effects due to a single line.

With the incident laser spectrum spread over an interval from 135 to 200 linewidths away from the $6 \leftarrow 0$ P(28) absorption line of Na_2, we observed a re-emission signal which is caused by proximity to this absorption line. While the separation from resonance suggests that the re-emission is resonant Raman scattering, we were unable to demonstrate this. This re-emission is enhanced over ordinary Raman scattering from N_2 by about 10^7. Careful quenching experiments should be able to determine whether this is resonant Raman scattering.

REFERENCES

1. D. G. Fouche and R. K. Chang, Phys. Rev. Lett. 29, 536 (1972).

2. R. L. St. Peters, S. D. Silverstein, M. Lapp, and C. M. Penney, Resonant Raman Scattering or Fluorescence in I_2 Vapor?, to be published in Phys. Rev. Lett.

3. C. M. Penney, L. M. Goldman, and M. Lapp, Nat. Phys. Sc. 235, 110 (1972).

4. Austin L. Wahrhaftig, J. Chem. Phys. 10, 248 (1942).

5. R. W. B. Pearse and A. G. Gaydon, The Identification of Molecular Spectra, Third Edition, Chapman & Hall, Ltd., London, 1963.

6. Gerhard Herzberg, Molecular Structure and Molecular Spectra, vol. 1, Spectra of Diatomic Molecules, Second Edition, Van Nostrand Reinhold Company, New York, 1950.

7. A. E. Wechsler, Characteristics of Metal Vapor, final report to Aerospace Research Laboratories, Contract No. AF33(657)-11735, for Arthur D. Little, Inc., 1966.

8. M. Lapp and L. P. Harris, J. Quant. Spectrosc. Radiat. Transfer 6, 169 (1966).

9. J. A. Paisner, K. S. Harvey, M. S. Sorem, and A. L. Schawlow, Bull. Am. Phys. Soc., Nov. 1972, p. 1128.

10. R. L. St. Peters and S. D. Silverstein, Manifestation of Pressure Broadening on Tuned Resonance Raman Fluorescence, to be published in Optics Communications.

11. Jeffrey I. Steinfeld and William Klemperer, J. Chem. Phys. 42, 3475 (1965).

APPENDIX C

INJECTION NARROWING OF A FLASHLAMP-PUMPED DYE LASER OSCILLATOR

GENERAL ELECTRIC

GENERAL ELECTRIC COMPANY
CORPORATE RESEARCH AND DEVELOPMENT
Schenectady, N.Y.

INJECTION NARROWING OF A FLASHLAMP-PUMPED DYE LASER OSCILLATOR

by

W.W. Morey
Physics and Electrical Engineering Laboratory

Report No. 73CRD043 January 1973

TECHNICAL INFORMATION SERIES

CLASS 1

GENERAL ELECTRIC

General Electric Company
Corporate Research and Development
Schenectady, New York

TECHNICAL INFORMATION SERIES

AUTHOR	SUBJECT	NO. 73CRD043
Morey, WW	lasers	DATE January 1973
TITLE Injection Narrowing of a Flashlamp-Pumped Dye Laser Oscillator		GE CLASS 1
		NO. PAGES 13
ORIGINATING COMPONENT Physics and Electrical Engineering Laboratory		CORPORATE RESEARCH AND DEVELOPMENT SCHENECTADY, N.Y.

SUMMARY

A high average power, narrow linewidth, and tunable dye laser is required for applications to remote probing of the atmosphere by any of several resonance spectroscopy techniques. The requirement of efficient high average power output is not easily made compatible with a narrow linewidth, however. In this report we examine a particular approach, injection narrowing of a high power oscillator, and compare it to other possible methods for obtaining a high power output with narrow linewidths.

The output from a low power, narrow linewidth, and tunable dye laser was injected into the resonating cavity of a high power broad band dye laser oscillator. For injected powers much greater than the fluorescence power generated into the resonator modes, the high power oscillator condenses its output spectrum to that of the injected laser field. This injection narrowed oscillator is compared to a high power oscillator that is directly narrowed with intracavity wavelength dispersive devices and to a conventional oscillator-amplifier system. It is concluded that for linewidths on the order of 10^{-3} nm or less the injection narrowing technique is preferred, but for linewidths greater than about 10^{-2} nm the other two systems appear to be more practical. Three different designs for efficient injection narrowing are recommended.

KEY WORDS

lasers, dye lasers

INFORMATION PREPARED FOR _____

Additional Hard Copies Available From

Corporate Research & Development Distribution
P.O. Box 43 Bldg. 5, Schenectady, N.Y., 12301

Microfiche Copies Available From

Technical Information Exchange
P.O. Box 43 Bldg. 5, Schenectady, N.Y., 12301

RD-54 (10/70)

INJECTION NARROWING OF A FLASHLAMP-PUMPED DYE LASER OSCILLATOR*

I. INTRODUCTION

The tunable flashlamp-pumped dye laser; for which output energies of up to 12J have been reported[1], offers a possible laser system to meet the requirements for remote atmospheric probing and undersea illumination. For more effective use of resonance fluorescence (RF) or near resonance Raman scattering (NRRS) phenomena in remote probing applications, not only must the bandwidth and stability of the probe laser be on the order of the absorbing linewidths of the species to be examined (typically on the order of 10^{-3} nm), but also maximum beam power is required. These two requirements, a narrow line at high power, are usually incompatible.

If a relatively high flashlamp pumping rate is used in order to obtain useful output power, then threshold is exceeded over a broader spectral region and a broad band output is obtained. To obtain a narrow linewidth requires wavelength dispersive devices to be placed in the laser cavity which give rise to significant intracavity losses, and still fail to produce adequate narrowing at high power. Thus, the presence of lossy intracavity dispersive elements and the reduction in pumping rate required to obtain a narrow line emission prevents utilization of the full power capability of the laser.

A. J. Gibson[2], for example, designed a flashlamp pumped dye laser for atmospheric probing with a spectral linewidth of 5×10^{-3} nm by using three Fabry-Perot etalons of successively smaller free spectral ranges. Gibson obtained a 10 mJ output pulse energy when the dye laser was operated broadband at 10 nm emission width with no etalons in the laser cavity. With the first etalon in the cavity the spectral width decreased to 0.3 nm and the pulse energy dropped 30%. Placing the second etalon in the cavity brought the spectral width down to 0.05 nm with a 50% decrease in the pulse energy, and when all three etalons were in the cavity Gibson obtained the 5×10^{-3} nm spectral width with 3 mJ output, a 70% decrease in the output pulse energy. This gives a net gain of 600 in the energy per unit wavelength, however.

* This research was supported by the Advanced Research Projects Agency of the Department of Defense and was monitored by ONR under contract No. N0014-72-C-0503.

Manuscript Received 1/30/73

Another approach to a laser transmitter for remote probing would be to amplify a low power frequency-narrowed-and-stabilized dye laser with a high power amplifier. However, this is not an efficient way to obtain the large pulse energies and narrow linewidths required. For low input power the amplifier is operating in the small signal amplifying regime, and a large amount of the amplifier pump light is going into fluorescence rather than stimulated emission. Using published results for maximum unsaturated gain of a flashlamp-pumped dye laser with rhodamine 6G[2], one can estimate the small signal gain of a high power commercial dye laser whose active length is 23 cm to be about 8.4 db per pass. Thus, the 3 mJ output of a single moded dye laser would be amplified to about 21 mJ. This commercial dye laser however, is capable of emitting 2J of laser energy in about 1μs when operated as an oscillator with broadband reflectors.

Another approach to obtain a narrow spectral output from a high power dye laser is to use injection narrowing. Here a low power spectrally narrow radiation field is injected into the optical resonating cavity of a high power dye laser oscillator at the time the laser is triggered. If the density of the injected photons in one or more of the cavity modes is considerably larger than the density of photons from spontaneous emission in all the cavity modes then the laser oscillation preferentially builds up on the injected radiation field rather than from the spontaneous emission noise, as is the usual case when the injected field is not present. This narrowing technique depends in part on the spectral broadening of the dye being homogeneous, so that the desired modes are in gain-competition with all the undesired modes. In practice this is found to be true to a high degree. The high power oscillator, then, can be made to lock its oscillation to an injected radiation field that has built up in the resonating cavity modes. In this way the high power laser emission can have the same spectral and beam divergence qualities as the injected radiation.

Injection narrowing was first demonstrated by Erickson and Szabo[4] with an N_2-laser-pumped dye laser and a pulsed argon laser. They reduced the spectral width of the dye laser from 40 to 0.00016 nm with the injection of 50 mW of 514.5 nm argon laser light. With 0.5 watts of injected power about 80% of the dye laser energy was spectrally condensed into the narrow line with the remaining 20% staying in the wings. The spectral intensity in the narrow line is thus 2×10^5 times that in the wings. Injection narrowing

has also been observed with a cw He-Ne laser as the injection source for a laser-pumped dye laser[5]. Recently G. Magyar and J.J. Schneider-Muntau used a 10^{-2} nm, 55 mJ, flashlamp pumped dye laser to injection narrow a high energy flashlamp pumped dye laser[6]. They obtained at least 90% of the total energy of the system in a single line about 10^{-2} nm wide. The effective energy gain or ratio of the final output energy of the injected high power oscillator to the total energy output of the low power injection laser was 200. When the system was used as a conventional oscillator-regenerative amplifier as in Ref. 6 an effective energy gain of only 2.5 was obtained.

The injection narrowing technique has the advantage of allowing one to use a convenient low power*, frequency-narrowed-and-stabilized dye laser to cause oscillation of a high power dye laser to occur with the same spectral quality as the injection laser. In this way a large fraction of the high power output obtained in broad band operation can be placed in the emission width of the injected laser beam. Potentially, then, this process could be more efficient than directly narrowing a high power oscillator with dispersive elements or using an oscillator-amplifier combination. In the next section we will describe our injection laser experiments, and then in the following section make a comparison of injection narrowing with the other aforementioned methods for obtaining a large energy per pulse with narrow spectral emission.

* By low power dye laser we mean one whose pumping rate does not exceed the threshold pumping rate to a large extent as compared to one that is driven to several times the threshold rate for maximum power output.

II. INJECTION-NARROWING STUDIES

The injection-narrowing experiments reported here utilized a low power, 3μs-long pulse, flashlamp-pumped dye laser to injection-narrow a Candela model SD625 coaxial flashlamp dye laser that is capable of emitting 2 joules in a 1μs pulse width. Since flashlamp-pumped dye lasers are usually triggered by spark gaps, synchronization of two lasers whose rise times are a small fraction of a microsecond would be erratic because of the inherent jitter present in the triggering spark gaps. By using a longer 3μs pulse for the injection laser, the submicrosecond jitter in the triggering is no longer a problem and synchronization can be achieved on nearly every shot.

The injection laser is spectrally narrowed using a 1200 ℓ/mm diffraction grating and a resonant reflector to form the laser cavity. The resonant reflector was constructed by coating both sides of a thin parallel glass plate with a 50% reflecting dielectric coating. The maximum reflectivity of the resonant reflector at its selected wavelengths would be more than 80%. When the injection laser is pumped about 20% over the threshold pumping rate, its emission consists of one to three lines whose widths are near 0.1 nm. The separation of these lines, determined by the free spectral range of the resonant output reflector, is 0.48 nm.

Figure 1 shows the experimental set up used to examine injection narrowing of the Candela laser. The dye used in these experiments was rhodamine 6G and the center wavelengths were around 590 nm. Referring to Fig. 1, the injection laser, whose beam is represented by the broken line, has a diameter about 3 mm at the exist of the laser. This beam diameter is expanded by a factor of 10 times in order to fill the 16 mm diameter aperture of the Candela laser. About 35% of the expanded beam is reflected from a beam splitter and sent along the optic axis of the Candela laser. The output reflector of the Candela transmits 75% of the incident injection laser beam and allows the injection laser's radiation to build up in the lasing cavity.

The two lasers are triggered with a combination Tektronix 162 waveform generator and two 163 pulse generators. Each pulse generator sends out a trigger pulse that can be delayed relative to the other in order to synchronize the flashlamps so the short pulse of the Candela laser occurs near the peak of the injection laser's output. To meet this condition it is

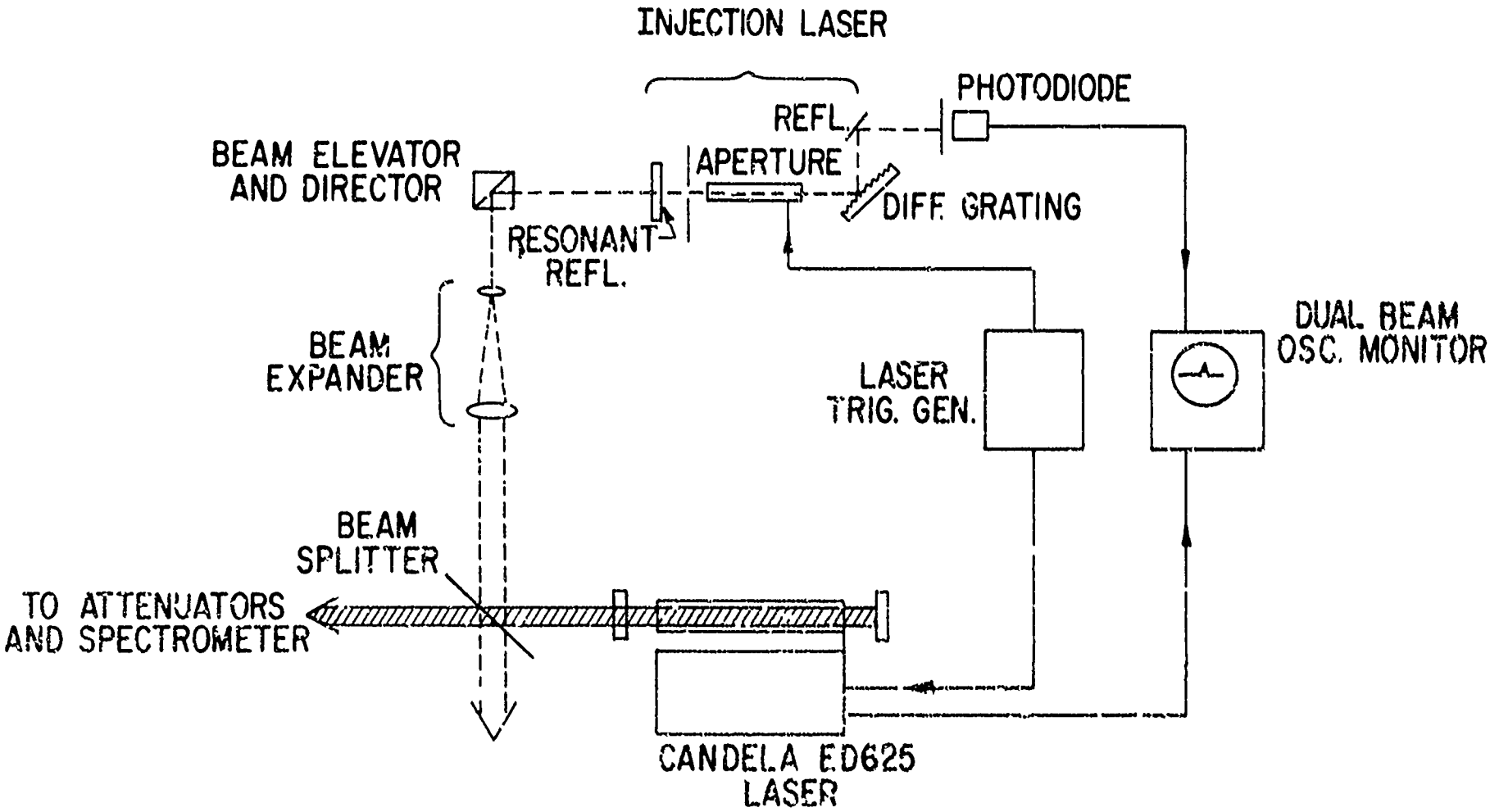

Fig. 1 Injection laser set-up.

necessary to delay the trigger to the Candela laser by about 13μs relative to the injection laser trigger signal. The injection laser is monitored with a PIN 10 photodiode by detecting the laser signal from the zero order reflection of the diffraction grating. This signal is displayed on a dual beam oscilloscope along with a flashlamp current monitor signal from the Candela laser. In this way one can set and check the synchronization of the lasers from shot to shot.

The Candela laser was aligned with a He-Ne alignment laser and then the expanded injection laser beam was aligned colinearly with the He-Ne laser beam. After passing through the beam splitter, the Candela laser beam, represented by the hashed arrow, was attenuated by reflection from a wedged glass plate and then with a Kratten neutral density 2.0 filter. The beam was then sent to a Jarrell-Ash 1 meter Czerny-Turner spectrograph where a spectrogram of the Candela laser was taken on Polaroid type 55 positive/ negative film. The resolution of the spectrograph is about 4×10^{-2} nm.

Spectrograms were made under different conditions where the lasers were synchronized or unsynchronized, one or the other laser blocked to prevent oscillation, and both lasers unblocked. When the lasers were out of synchronization and unblocked only the broad band emission of the Candela laser was recorded on the film. In this case the much lower intensity of the injection laser that was reflected back from the Candela mirrors was not enough to expose the film. When the lasers were brought into proper synchronization, however, injection narrowing was easily observed since the much narrower emission linewidth of the injection laser was predominant on the film.

Figures 2, 3, and 4 were made by taking microphotometer traces from the Polaroid negative film. The vertical axes in these figures can be related to the intensity of the incident light in one portion of the output beam. Using a calibrated step attenuating film to check the microphotometer, however, it was determined that the ordinate is not a linear scale in intensity and to preserve the proper relation between low intensity and high intensity portions of the traces, the high peaks in Figs. 3 and 4 should be about 30% higher than shown. The horizontal axis, of course, represents wavelength with the scale shown in Fig. 2.

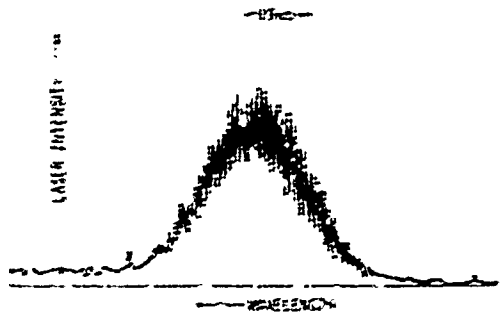

Fig. 2 Output spectrum of the Candela laser with no injection.

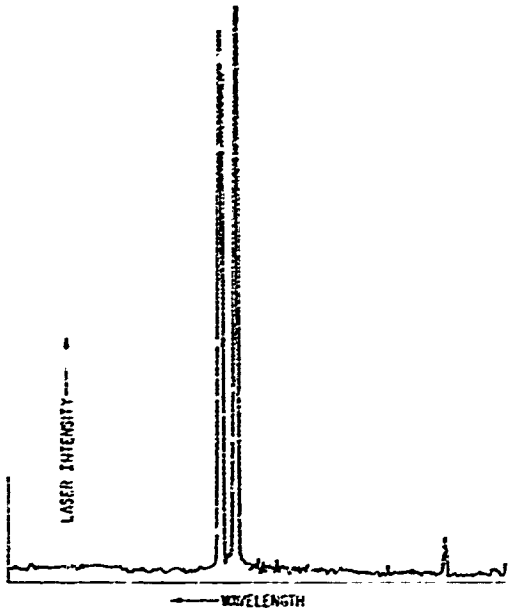

Fig. 3 Output spectrum of the Candela laser with injection.

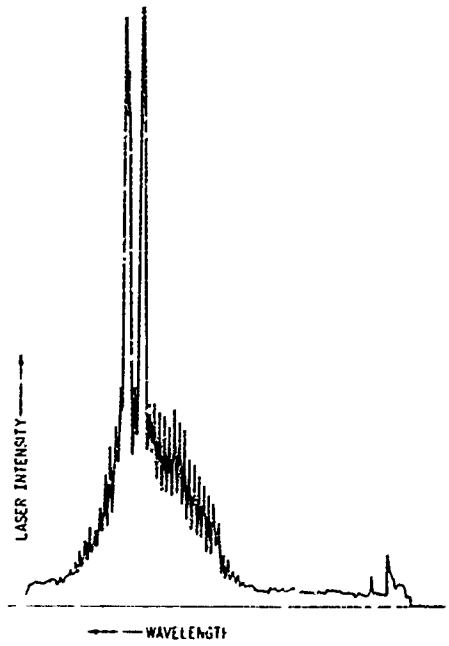

Fig. 4 Partial locking of the Candela laser spectrum with injection.

Figure 2 shows the output of the Candela laser alone. The bandwidth of the emission is around 4.0 nm. It can be seen from Fig. 2 that the emission spectrum is modulated to a fairly high degree. This is caused by interfering reflections in the resonating cavity from the windows of the optical cell that contains the flowing dye solution. The Candela laser in this instance was emitting about 0.8[illegible]. Figure 3 shows the result under identical conditions as those of Fig. 2 except that the injection laser is unblocked and synchronized with the Candela laser. In Fig. 3 we see the emission spectrum is that of the injection laser but the beam energies are of the order of those of the Candela laser. The Candela laser, then, has essentially locked its output to the injection laser's spectrum. The two emission peaks represent two modes of the injection laser's resonant reflector and are separated by 0.48 nm. There is also a barely resolvable fine structure contained in each of the two emission peaks. This is caused by interfering reflections from the dye cell windows of the injection laser. A microphotometer trace made at a slower speed more clearly resolves the structure in these emission peaks and shows that the longer wavelength peak contains 4 subpeaks of which the third subpeak is reduced about 30% from the other 3 subpeaks. The amount of reduction of the third subpeak and its spacing relative to the first subpeak agrees with the modulation depth and spacing of the Candela laser modulation as observed in Fig. 2. In another spectrogram taken at a slightly different wavelength one of the two main peaks has only one subpeak and a half width of about 5×10^{-2} nm. This is about the resolution of the spectrometer so the actual emission width in this case was somewhat smaller.

Considering the losses of the beam elevator and director, the beam expander lenses, and the fraction reflected by the beam splitter, about 22% of the injection laser's output is directed towards the output reflector of the Candela laser. This output reflector transmits 75% of the incident beam allowing the injected radiation to build up within the Candela resonator cavity. The smaller bore diameter of the Candela laser with respect to the expanded injection laser beam diameter reduces the injection power by an additional factor of 27.4%. The injection laser power transmitted into the Candela laser cavity, then, is about 4.7% of the output of the injection laser. The PIN 10 photodiode, used to monitor the injection laser, was calibrated by simultaneously measuring the output power with a calibrated

ITT vacuum photodiode and diffuse reflector. For the spectrogram in Fig. 3 the PIN 10 diode monitor indicated that the injection laser was generating about 230 watts at the time the Candela laser fired. In this instance, then, the injected laser power sent into the Candela laser cavity would be about 11 watts. For a comparison we can estimate the amount of fluorescence power generated in the laser cavity modes by considering the fluorescence emitted into the solid angle of the laser beam. Estimations of the conversion efficiency of electrical power driving the flashlamps to light power absorbed by the dye laser pump bands, the quantum efficiency for fluorescence, and the shift in wavelength from absorption to fluorescence gives a factor of about 0.3% for the conversion of pumping power to fluorescence power. This conversion efficiency is slightly greater than the measured 0.27% laser efficiency at the 300 MW peak pumping level used for Figs. 2, 3, and 4. The threshold pumping rate was found to be 90 MW. Therefore at this pumping rate we would have 0.27 MW of fluorescence power. Since the fluorescence radiates into 4π steradians, we can estimate the amount of fluorescence that is radiated into the cavity resonator modes by considering the fraction of the total solid angle included in the laser divergence angle. Allowing for two directions of emission and a divergence angle of 2.5 mrad, we get a fraction of 0.78×10^{-6}. Multiplying this fraction by the 0.27 MW we obtain 0.2 watts of fluorescence generated into the Candela resonator modes near the threshold of oscillation. This is more than an order of magnitude less than the injected laser power sent into the resonator and causes the Candela laser to emit practically all of its energy into that part of the injection laser's spectrum that builds up in the resonator cavity modes. Spectrograms taken where the injection laser power was several times smaller shows a considerable amount of broad background radiation. In this case the laser was only partially locked to the injection laser spectrum. A case like this is shown in Fig. 4. From this figure it appears as though the injected signal depletes the long wavelength side of the Candela spectrum. It is also interesting to note that injection locking can be observed even when the injection laser's emission lines are shifted in wavelength to lie outside the natural emission wavelength of the Candela laser. In this case lasing action is observed at a wavelength which without injection would lie below threshold.

III. CONCLUSIONS

These experiments confirm that a relatively small amount of injection power can control the spectral distribution of much larger power levels produced by a dye laser oscillator. Many spectrograms have been taken with the injection laser system described above with different pumping energies and injected power levels. They show that the injected field must compete with the fluorescence power generated in the oscillator resonator modes; and a minuscule amount of injected power in a high power oscillator will not lock the oscillator to the spectrum of the injected field. The injected power requirement for locking the oscillator is relatively small; in the results demonstrated above 11 watts was more than sufficient to lock the oscillator driven by 300 MW of flashlamp pumping. Even though injection narrowing of a high power oscillator does offer a very attractive alternative to direct frequency narrowing techniques and oscillator-amplifier combinations, 100% utilization of the output capabilities of the laser cannot be made because some output power must be sacrificed from the oscillator in order to be able to inject the field of the frequency narrowed laser. In our experiment this loss came from the beam splitter that was placed external to the oscillator cavity. In practice, however, this loss could be reduced to a few percent by choosing appropriate reflecting optics for the beam splitter and properly matching the beam sizes.

One could, for example, use a Brewster angle reflector as shown in Fig. 5a to reflect the injection laser beam along the optic axis of the oscillator. The reflected beam could then be sent through a 45° rotator and then into the oscillator. The oscillator output would lock to the polarization of the injected beam and, traveling in the opposite direction, its output would be rotated an additional 45° and transmitted by the Brewster angle reflector. The losses in this case would just be the losses of the rotator. Another scheme that is very attractive is shown in Fig. 5b. In this case the output reflector of the injection laser is also used as the high reflectivity reflector of the oscillator. The loss to the high power oscillator would be in the reduction in the reflectivity of its mirrors required for injecting the tuned laser. The beam expander in Fig. 5b matches the small beam diameter of the injection laser to the larger diameter of the high power oscillator and makes the tilted etalon more effective in frequency narrowing. By placing the injection laser at an appropriate

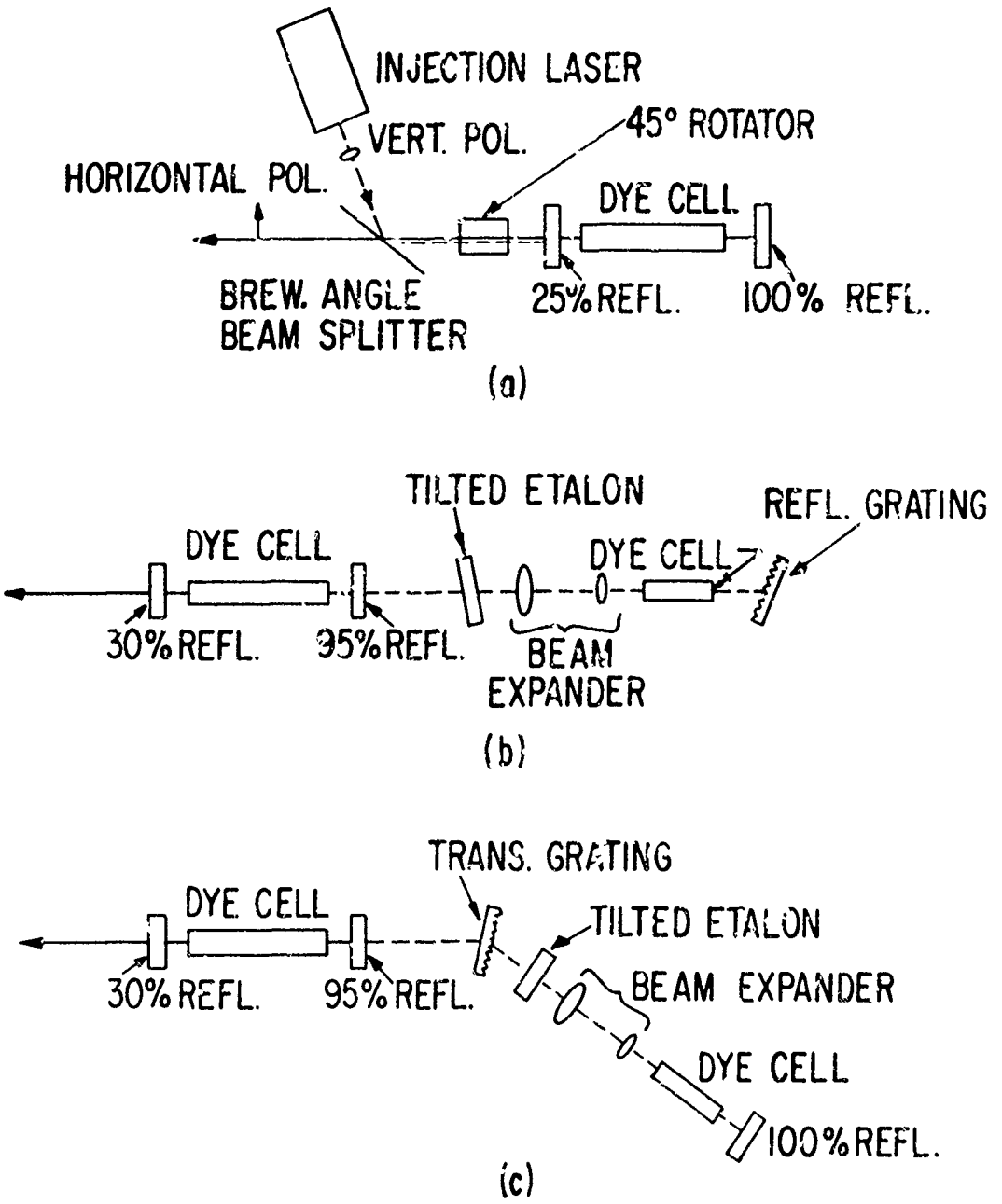

Fig. 5 Injection laser systems design

(a) using a Brewster angle plate for efficient injection,

(b) using a common reflector and a reflection grating, and

(c) using a common reflector and a transmission grating.

angle relative to the oscillator, a transmission type diffraction grating could be used after the tilted etalon as shown in Fig. 5c. This would make better use of the beam expander for frequency narrowing. For this case a 100% reflector would replace the reflection grating of Fig. 5b.

In comparing the efficiency of an injection narrowed laser system with a narrowed oscillator system consideration must be made of the additional energy required to drive the low power injection laser. For example, if a linewidth requirement is only 0.3 nm, direct frequency narrowing of an oscillator will decrease the broadband output by only about 30%. Using injection narrowing, one would be capable of achieving the same linewidth with only a few percent reduction in the oscillator output capabilities; but, of course, this would require another laser with additional power consumption. In this case direct frequency narrowing of an oscillator would be advantageous. On the other hand, for very narrow emission widths on the order of 5×10^{-3} nm or less, the reduction in output capability with direct narrowing becomes 70% or more, and injection narrowing becomes an attractive alternative to direct frequency narrowing.

In order to achieve the output power levels with narrow linewidths which can be reached by injection narrowing of a high power oscillator, a conventional low power oscillator plus multistage amplifier system would have to work under small signal gain conditions for most of the amplification process. Not only is the small signal regime intrinsically very inefficient for power amplification, but also the losses associated with a multiplicity of amplifier stages (or multipassing a single stage) and the losses to fluorescence when operating in the small signal amplification regime would combine to make the conventional oscillator-amplifier approach impractical.

In summary, then, it has been demonstrated that injection narrowing is a realizable approach to obtaining high power and energy per pulse with a spectrally narrow and tunable output. For linewidths on the order of a few tenths nanometer or more, direct narrowing of the oscillator with dispersive elements in the laser resonator cavity is the best approach. However, for narrower linewidths as required for resonance scattering (on the order of a few thousandths of a nanometer), or possibly for lower beam divergence qualities, the injection laser technique appears to be the best approach.

ACKNOWLEDGMENTS

The author would like to thank Drs. D.J. Taylor, D.R. White, and R.L. St. Peters for helpful discussions and assistance in preparing the report.

REFERENCES

1. P. Anliker, M. Gassman, and H. Weber, "12 Joules Rhodamine 6G Laser" Opt. Comm. 5, 137 (1972).

2. A. J. Gibson, "A Flashlamp-Pumped Dye Laser for Resonance Scattering Studies of the Upper Atmosphere" J. Sci. Inst. (Jour. of Phys. E) 2, 802 (1969).

3. B. G. Huth and M. R. Kagan, "Dynamics of a Flashlamp-pumped Rhodamine 6G Laser" IBM Jour. Res. Dev. 15, 278 (1971).

4. L. E. Erickson and Szabo, "Spectral Narrowing of Dye Laser Output by Injection of Monochromatic Radiation Into the Laser Cavity," Appl. Phys. Lett. 18, 433 (1971).

5. Q. H. F. Vrehen and A. J. Breimer, "Spectral Properties of a Pulsed Dye Laser With Monochromatic Injection," Optics Comm. 4, 416 (1972).

6. G. Magyar and H. J. Schneider-Muntau, "Dye Laser Force Oscillator," Appl. Phys. Lett. 20, 406 (1972).

APPENDIX D

THE DYE ZIG-ZAG FACE-PUMPED LASER: A HIGH AVERAGE POWER, HIGH BRIGHTNESS LASER

GENERAL ELECTRIC

GENERAL ELECTRIC COMPANY
CORPORATE RESEARCH AND DEVELOPMENT
Schenectady, N.Y.

THE DYE-ZIG-ZAG-FACE-PUMPED LASER: A HIGH AVERAGE POWER HIGH BRIGHTNESS TUNABLE LASER*

by

R. L. St. Peters and D. J. Taylor
Physics and Electrical Engineering Laboratory

Report No. 73CRD059 February 1973

TECHNICAL INFORMATION SERIES

*This research was supported by the Advanced Research Projects Agency of the Department of Defense and was monitored by ONR under Contract No. N0014-72C-0503.

CLASS 1

GENERAL ELECTRIC

General Electric Company
Corporate Research and Development
Schenectady, New York

TECHNICAL INFORMATION SERIES

AUTHOR	SUBJECT	NO.
St. Peters, RL Taylor, DJ	tunable laser	73CRD059
		DATE: February 1973
TITLE: The Dye-Zig-Zag-Face-Pumped Laser: A High Average Power, High Brightness Tunable Laser*		GE CLASS: 1
		NO PAGES: 33
ORIGINATING COMPONENT: Physics and Electrical Engineering Laboratory		CORPORATE RESEARCH AND DEVELOPMENT SCHENECTADY, N Y

SUMMARY

Thermally induced distortion, one of the important average-power-limiting factors in dye lasers, has been eliminated by the use of the General Electric Zig-Zag-Face-Pumped Laser configuration with transverse dye flow. The model described in this report has produced an output power of 1 watt with an overall efficiency of 0.04% using unpurified commercial dye and no quenchants other than oxygen. The limit on its output is in the pulsing circuitry, not thermal distortion. Efficiency is limited by the inability to use the full 9 cm^2 aperture as an oscillator. Measurements of the performance both as an amplifier and an oscillator are in good agreement with detailed theoretical analysis, and this analysis indicates that both the output and efficiency can be readily increased in future more nearly optimal versions.

*This research was supported by the Advanced Research Projects Agency of the Department of Defense and was monitored by ONR under Contract No. N0014-72C-0503.

KEY WORDS

tunable laser, dye laser, high-power laser

INFORMATION PREPARED FOR _____

Additional Hard Copies Available From

Corporate Research & Development Distribution
P.O. Box 43 Bldg. 5, Schenectady, N.Y., 12301

Microfiche Copies Available From

Technical Information Exchange
P.O. Box 43 Bldg. 5, Schenectady, N.Y., 12301

RD-54 (10/70)

THE DYE-ZIG-ZAG-FACE-PUMPED LASER:

A HIGH AVERAGE POWER, HIGH BRIGHTNESS TUNABLE LASER*

R.L. St. Peters and D.J. Taylor

I. INTRODUCTION

Dye lasers, which use an organic fluorescent dye in a liquid solution as the active medium, are the most important tunable lasers operating in the visible portion of the spectrum. This spectral region plus part of the near IR can be continuously covered using only a few dyes, and frequency doubling techniques extend the tuning range to at least 250 nm in the near uv.

One of the important limitations on the average power capability of dye lasers is the distortion caused by thermally induced inhomogeneities in the dye solution. The dye Zig-Zag-Face-Pumped Laser (DZZ-FPL) configuration reduces these inhomogeneities by uniform pumping of the dye solution and by rapid circulation of the dye solution through the active region. Furthermore, the optical configuration is such that the residual distortions are largely self-canceling, resulting in a very small net distortion.

We have constructed and tested a prototype DZZ-FPL in order to determine optimum design parameters, to establish a basis for predicting the performance of future DZZ-FPL designs, and to demonstrate the low distortion properties and high average power potential. With one kilowatt average input power at two pulses per second, no distortion was observed. We have achieved average output power of 1W at 3 pps. The low efficiency of 0.04% is a result of the particular configuration; higher efficiencies and outputs for the same input are possible.

* This research was supported by the Advanced Research Projects Agency of the Department of Defense and was monitored by ONR under Contract No. N0014-72-C-0503.

Manuscript Received 2/16/73

II. CONSTRUCTION

The core of the DZZ-FPL is a series of transparent prisms with channels between them, as illustrated in Fig. 1. This prism assembly is housed in a long glass box, which also encloses the dye reservoirs. The dye solution flows vertically through the channels and is optically pumped by two linear flashlamps, one along each side of the structure. The end prisms have faces perpendicular to the axis of the prism structure; this axis is also the optical axis of the DZZ-FPL. The lamps are enclosed in reflectors which direct the pumplight toward the dye in the channels. An end view diagram is shown in Fig. 2.

In order to contain the pump light within the dye channel-prism core until it is absorbed by the dye, the prisms are aluminum coated on the top and bottom. These coated surfaces and the lamp reflectors form a nearly continuous reflective cavity open only at the ends and at the necessary holes for dye flow, lamp electrodes, etc. Since aluminum coatings come off when bathed in the dye solution particularly under pumplight illumination, the aluminum was overcoated with SiO, and the prisms were then baked in air at 300°C for 18 hours. The aluminum coatings resulting from this treatment proved quite durable but still showed some degradation during the DZZ-FPL + ting, perhaps due to small holes in the overcoat.

In order to keep the loss due to absorption in the prisms low, the prisms were made from Dynasil 8000 grade low schlieren fused silica selected for freedom from bubbles. The prisms were cut with the deposition planes of the material oriented perpendicular to the optic axis to further reduce schlieren distortion. The windows at the ends of the DDZ-FPL were made of BK-7 optical glass initially. Subsequently windows of fused silica with multi-layer dielectric anti-reflection coatings on the external surfaces were used, resulting in a substantial performance improvement as described later.

The optical aperture is 3 cm by 3 cm. Ten channels were used with various thicknesses as discussed below. The overall length of the core structure, which varied slightly with channel thickness, was approximately 30 cm.

The electrical circuit used for the single pulse measurements is shown in Fig. 3. Separate 3.5 μf capacitors for each lamp were charged by a single DC supply through 100 kΩ resistors. The lamp cathodes were connected to a common triggered spark gap in order to assure simultaneous firing of both lamps. This

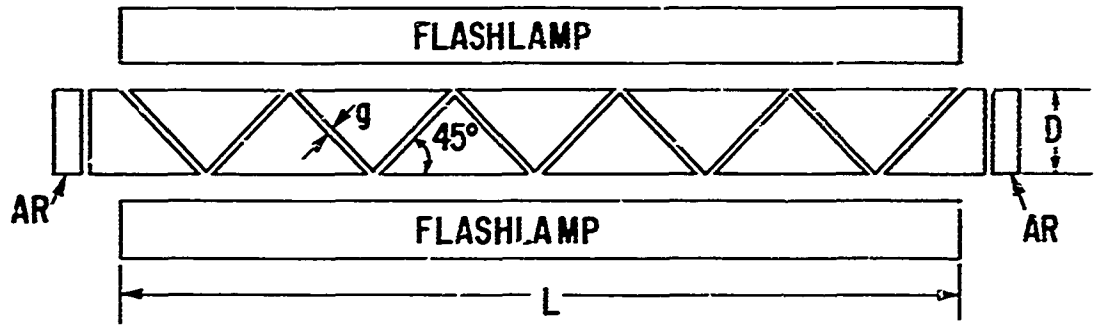

PRISM THICKNESS (NORMAL TO PAGE) = W

Fig. 1 Top view of Dye Zig-Zag-Face-Pumped Laser.

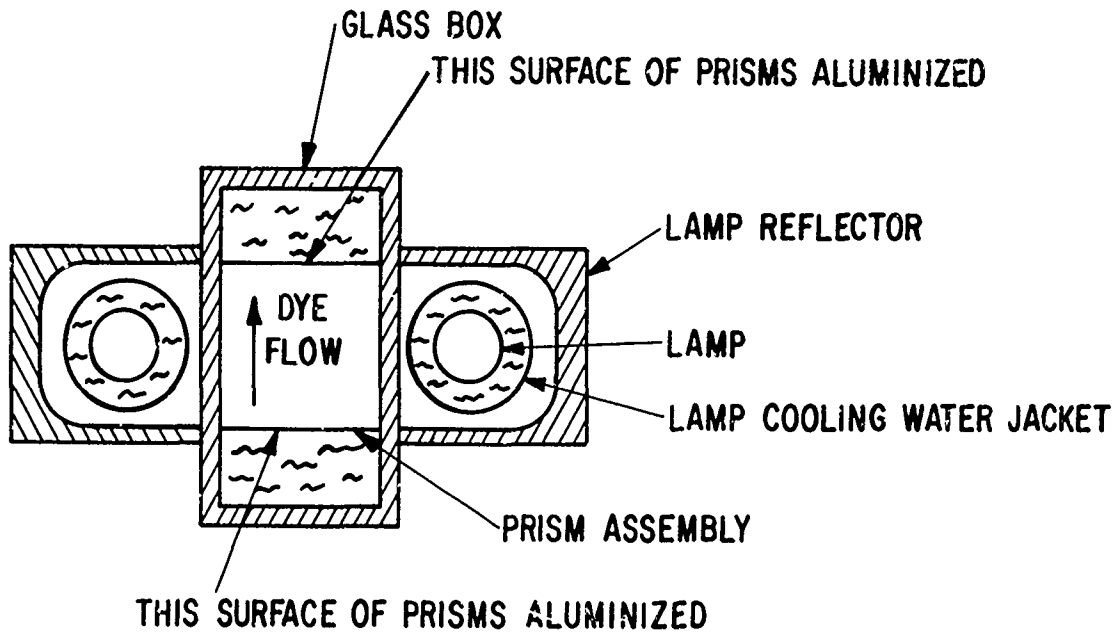

Fig. 2 End view of Dye Zig-Zag-Face-Pumped Laser.

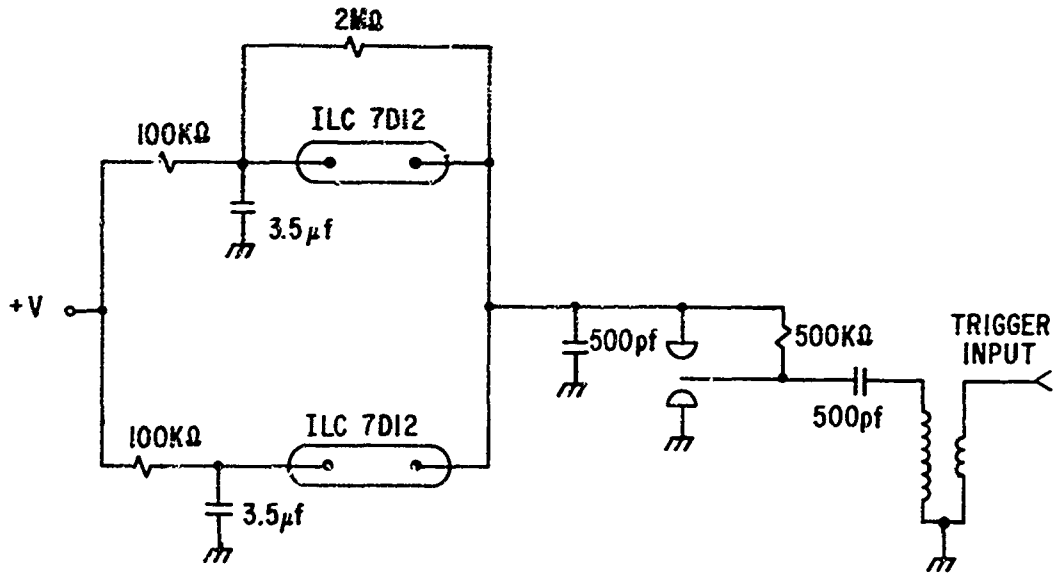

Fig. 3 Electrical circuit for puising DZZ-FPL flashlamps.

circuit was later modified for the gain and distortion measurements. Installation of separate spark gaps for each lamp reduced the jitter in the delay between triggering and lamp firing from typically 40 μsec to less than 1 μsec while still providing simultaneous firing of both lamps, so as to allow synchronization with an external oscillator for gain measurements. For the repetition rate measurements a Hipotronics power supply, capable of 2 amps at 15 kV, provided the charge on the 3.5 μf capacitors through two 15 kΩ resistors that were cooled by flowing transformer oil. With this supply the risetime to the 65% point of 140 msec (more than twice the expected RC charging time-constant of 52 msec due to an internal saturable reactor) effectively sets the maximum repetition rate at approximately 7 pps (the dye flow rate, discussed below, also limits this system to 7 pps.) Consistent firing at 5 pps was observed with virgin lamps and freshly cleaned spark gaps.

The dye flow arrangement in the DZZ-FPL is shown in Fig. 4. Two inlets on the bottom and two outlets on the top were used. The inlet at one end and the outlet at the other end were partially restricted by a section of smaller diameter tubing. This arrangement was necessary to assure a good dye flow through each channel. A pump circulated the dye through the DZZ-FPL, a dye reservoir, a heat exchanger, and a coarse filter. Tap water was circulated through the other heat exchanger chamber. The dye flow rate was approximately 90 ml/sec, so that exchanging the total volume of dye within the channels required 0.13 sec.

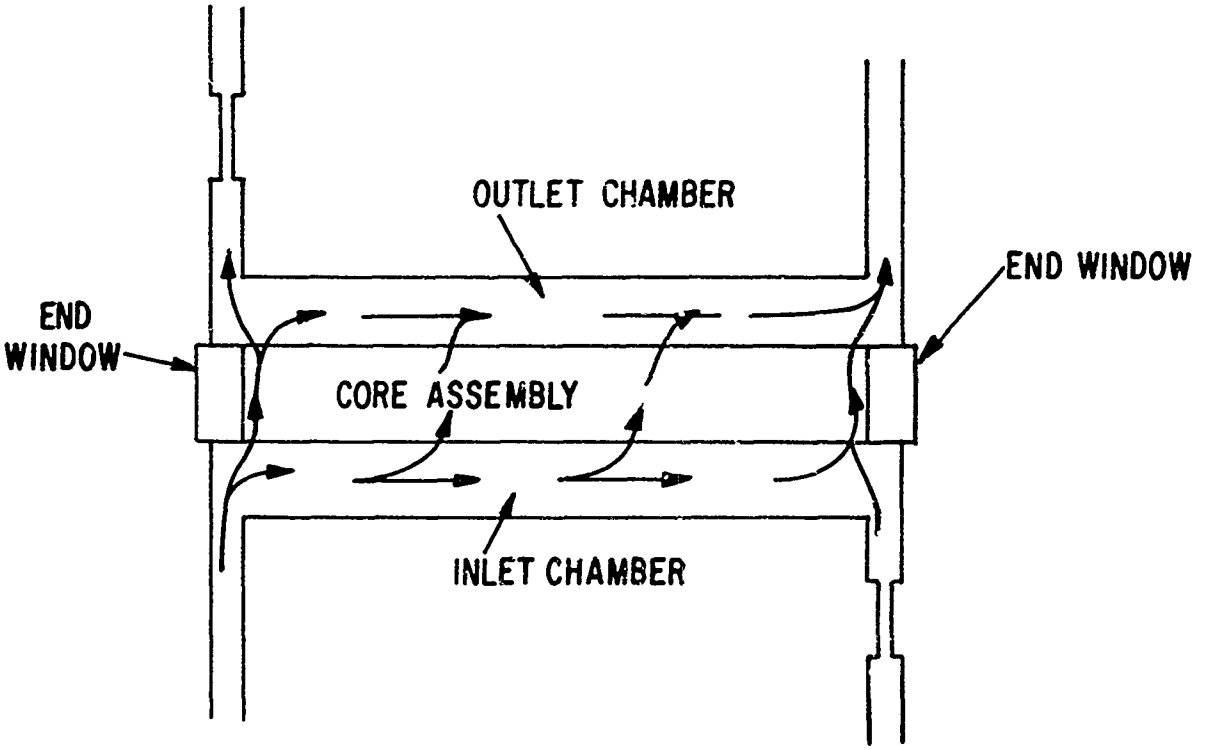

Fig. 4 Dye solution fluid flow pattern.

III. SINGLE PULSE MEASUREMENTS

A. Parameter Optimization

Early developmental work on the DZZ-FPL had used a version with channels 6.3 mm thick.[1] The optimum concentration of Rhodamine 6G in ethanol was found to be approximately 2×10^{-4} M. Observation of the flow of dye solution through this early version made it clear that thinner channels were desirable, since for example the solution tended to swirl about in the channels rather than flowing continuously through them. Use of narrower channels requires a higher concentration if the same number of dye molecules is to be maintained in the active volume. Substantially smaller channels require concentrations higher than those found in the literature and it was expected that at some point dye-solvent interactions or other concentration-dependent effects would reduce the performance. The first part of this investigation was to experimentally determine the minimum channel thickness and concentration at which the single pulse performance could be maintained.

For these measurements the DZZ-FPL was used as an oscillator since oscillator tests are simpler than amplifier tests. The cavity consisted of two mirrors, each 5 cm in diameter, spaced 77 cm apart. One mirror had a 5 m radius surface with a broadband high reflectivity coating, the other was flat with a transmission measured to be 18% at 595 nm, the measured wavelength at which lasing occurred. All tests were made using Rhodamine 6G in ethanol as the dye solution. The optimum concentrations for each of these channel widths were determined by threshold measurements, and it was also determined that these concentrations yielded the maximum output for a constant input pump level.

An ITT vacuum photodiode with an S-1 photocathode and a factory supplied sensitivity vs. wavelength curve was used to measure the energy output. The wavelength of oscillation was measured to be $\sim$ 595 nm using a small hand-held grating spectrometer and confirmed using interference filters. The output of the DZZ-FPL was incident on an approximately Lambertian surface whose scattering angle curve had been measured. This surface consisted of a layer of MgO about 6 mm thick covered with 2 thin layers of Eastman Kodak high reflectance paint. The detector was placed so that it viewed this surface at a known angle to the normal (near zero to minimize the sensitivity to uncertainty in the angle) and from a measured distance. The power incident on the detector was thus proportional to the output power,

$$P_d = P_o \frac{A_d}{\pi R^2} \cos \theta$$

where P_d = power at the detector,

P_o = laser output power,

A_d = detector area,

R = detector-scattering surface distance, and

θ = angle to scattering surface normal.

This equation assumes a Lambertian surface which is perfectly efficient (i.e., scatters all light incident on it with no absorption). Our surface was not exactly Lambertian nor perfectly efficient, but the deviations were small and nearly mutually canceling, making this equation a good approximation.

The output of the detector was stored on a capacitor. The voltage across this capacitor at any instant was thus proportional to the total energy incident on the detector up to that time. This voltage was observed on an oscilloscope, and a sharp rise could be seen when lasing occurred. At low output this sharp rise was superimposed on a slower rise caused by pump light and dye fluorescence; care was taken to subtract this contribution to the total detected energy. As a check, the capacitor was removed and the voltage across a resistor in series with the detector output was observed on the oscilloscope. This voltage was proportional to the instantaneous power at the detector. The energy was obtained from the area of the pulse. The laser pulse appeared as a short ($<2\mu$ sec) high pulse superimposed on the longer ($\sim 6\mu$ sec) low pump pulse. The two signals were more easily separated with this type of display. The results obtained for the laser pulse energies were in good agreement between these two methods.

For each channel thickness the output and slope efficiency were measured using the concentration which yielded the lowest threshold. The single pulse performance using the two larger channel thicknesses was essentially the same, while the performance with the thinnest channels was substantially worse. The performance data for these three cases are shown in Fig. 5 and in Table I. From Fig. 5 and Table I, it is clear that the performance of the DZZ-FPL is not much different using 0.91 mm channels and 1.17 mm channels. The apparent slight inferiority of the performance with 1.17 mm is probably not real and a result of some combination of the following:

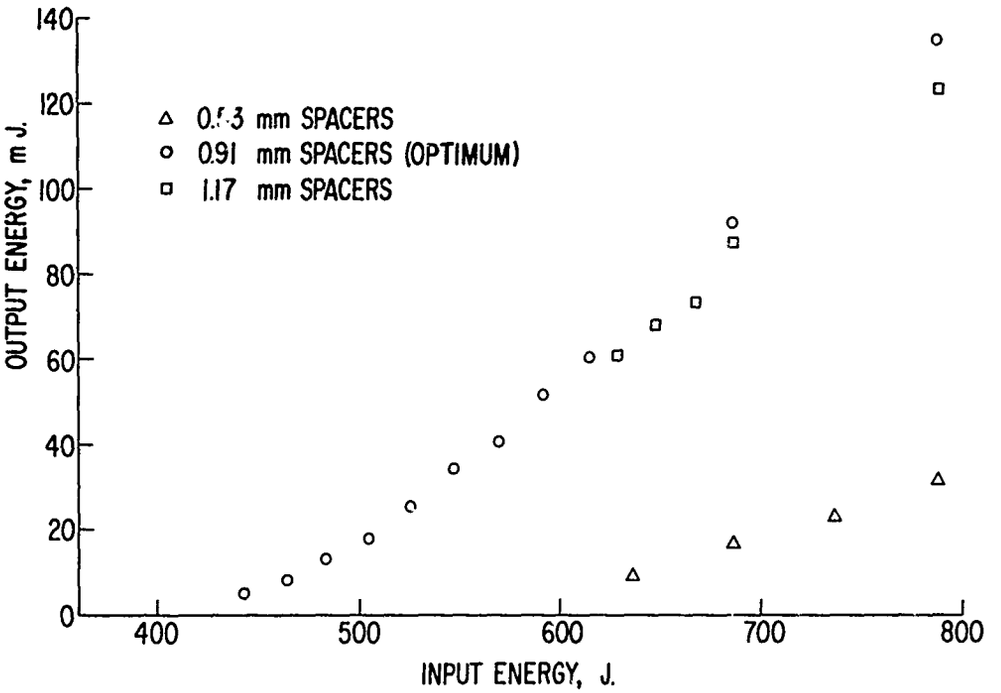

Fig. 5 Output energy as a function of input energy for three channel thicknesses.

TABLE I. DYE CONCENTRATION, THRESHOLD ENERGY,

AND SLOPE EFFICIENCY FOR THREE CHANNEL THICKNESSES.

Spacer Thickness mm	Optimum Conc. Molar.	Threshold J	Slope Efficiency %
0.53	1.5×10^{-3}	521	0.015
0.91	1.25×10^{-3}	397	0.043
1.17	5×10^{-4}	416	0.039

1. The 1.17 mm data were the last taken and the flashlamps may have been degraded.

2. The concentration may not have been optimal. The performance is not very sensitive to concentration over a range of a factor of 2 or 3 around the optimum concentration, making the optimum difficult to determine precisely. In particular, the optimum concentrations for 0.91 mm and 1.17 mm channels are probably not as different as Table I indicates.

3. There may have been slight differences in the mirror alignment or the positioning of the detector and diffuse reflector, since these measurements were separated by a number of days.

The performance with 0.53 mm channels, however, is degraded by a factor of 2 in slope efficiency and the threshold is 30% higher.

It is thus concluded that the optimum channel thickness (i.e., the smallest channel width at which the single pulse performance is not degraded) is near 0.9 mm and the corresponding optimum concentration is near 1.25×10^{-3} M.

These tests were performed before the fused silica anti-reflection coated end windows were available. The round trip absorption and reflection losses (excluding dye self-absorption) were found to total ~ 12% for this configuration. Thus the performance shown in Fig. 5 only indicates the relative performance of the various channel thicknesses. The performance available from the low loss version with optimum channel size and concentration is presented below.

B. Oscillator Output Power and Gain

Detailed studies of the Dye Zig-Zag-FPL as an oscillator and as an amplifier were made on the optimized DZZ-FPL configuration. Losses were reduced to a minimum by using prisms of fused silica, for which absorption and scattering losses are unmeasurably low, and fused silica end windows, which were anti-reflection-coated on the outside. The only remaining transmission losses are the dye self-absorption, Fresnel losses at the prism/dye interfaces (only 0.55% single-pass for the favored polarization), scattering losses at the surfaces, and any absorption by the solvent. The measured transmission loss at 632.8 nm (He-Ne), where dye self-absorption is negligible, was less than 2%. The 30 cm-long xenon flashlamps with 5 mm bore diameter used in the earlier experiments were replaced by 7 mm bore flashlamps, offering a more nearly optimum spectral

distribution and longer lamp life. For these studies the channel thickness was 0.91 mm and the concentration of dye in ethanol was 5×10^{-4} M, since it was found above that performance is not very sensitive to concentration within the range 5×10^{-4} to 1.25×10^{-3}M. The oscillator cavity configuration was the same as that described earlier, with an 18% transmitting output mirror, and oscillation occurred at a wavelength of about 595 nm.

The output energy from this DZZ-FPL oscillator was measured using the calibrated photodiode and integrating circuit that were described above. The single pulse laser output energy as a function of the energy stored in the capacitors is shown in Fig. 6. The threshold energy was 230 J, and a laser output of 0.22 J was obtained with 550 J pumping, for an overall efficiency of 0.040%. The region of slowly increasing output has also been observed in the operation of previous DZZ-FPL versions, and seems to be characterized by an increasing spot size (larger number of transverse modes oscillating). The slope efficiency in the linear region of 0.077% was nearly twice that obtained from the higher-loss version. The major factor in this increase was the 1.60 times higher output coupling efficiency due to the reduced transmission loss; the remainder of the slope efficiency improvement was due to higher spectral efficiency and other factors. The temporal behavior of the DZZ-FPL laser pulse essentially followed the lamp pulse except that it was somewhat shorter at both the rising edge and the falling edge due to the DZZ-FPL threshold. The lamp pulses were typically 8 μsec between half-power points, while the laser pulses were typically 5 μsec ± 1 μsec.

A convenient and accurate way to measure both the small-signal gain and the cold-cavity loss of a laser oscillator is to measure its threshold with and without an additional known cavity loss. For example, one of the cavity mirrors may be replaced by a mirror of higher transmission, or a device of known attenuation may be inserted into the cavity. Adopting the latter technique, we utilized the Fresnel reflections from a clean glass slide inserted at near normal incidence (sufficiently far from normal to avoid resonance effects). This additional round trip loss $\delta_s = 0.160$ caused threshold to rise from 241 to 333 J. From the expression E_{th} (slide)/E_{th} (no slide) = $[1-(1-\delta_o)(1-\delta_e)(1-\delta_s)]/[1-(1-\delta_o)(1-\delta_e)]$, where $\delta_e = 0.18$ is the transmission of the output mirror, we determine the round-trip cold cavity loss to be $\delta_o = 0.139$ or single-pass loss of 7.2%. The major contributions to the single-pass loss are the reflection loss, expected to be 0.55%,

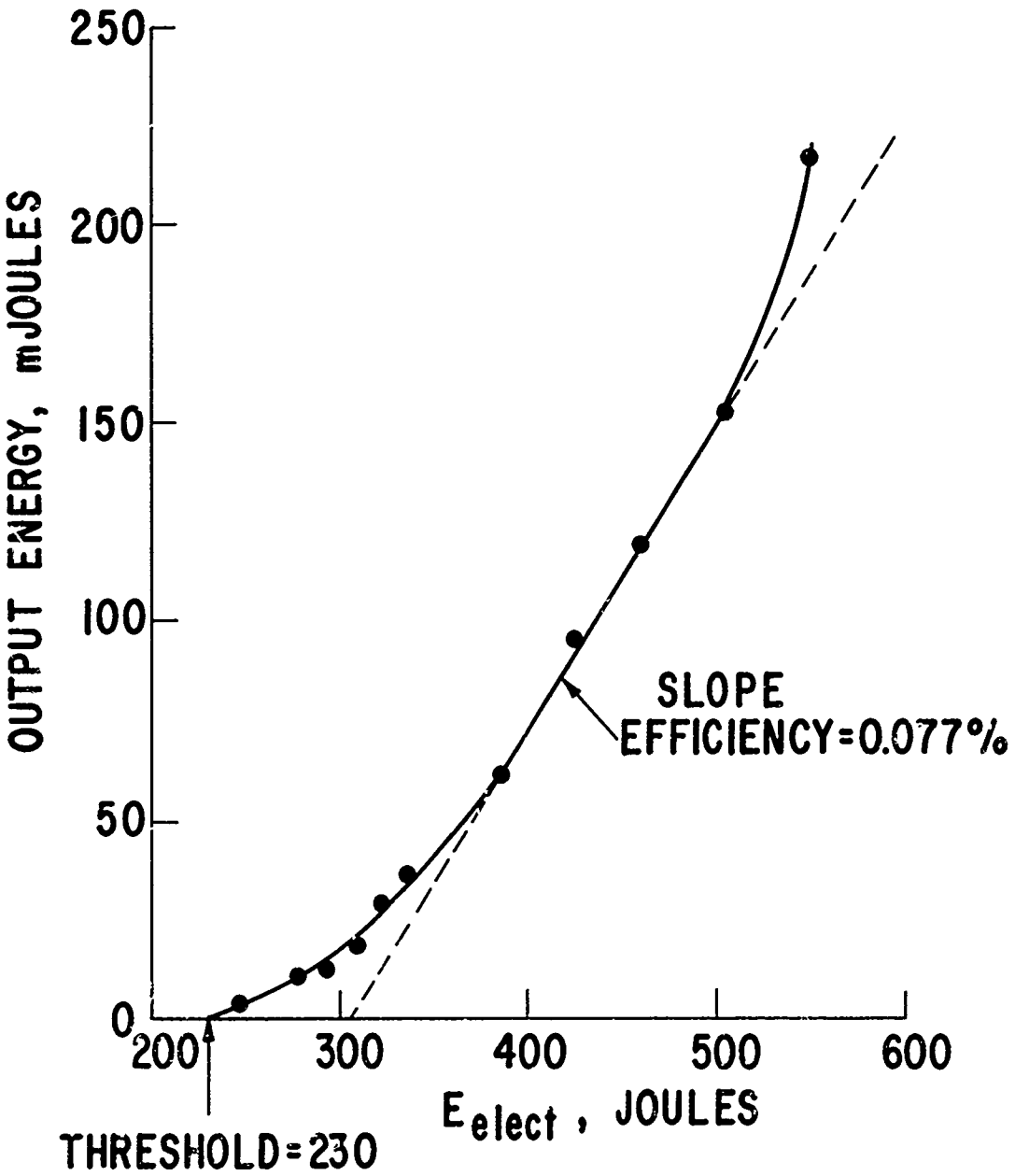

Fig. 6 Output energy of cptimized DZZ-FPL.

as discussed above, and dye self-absorption loss. This loss may be estimated from the absorption coefficient $\varepsilon \approx 0.15 \pm 0.05 \times 10^{-18}$ cm^2 given by Snavely's[2] Fig. 10 at λ_o = 595 nm. With dye concentration 5×10^{-4}M and dye length along the optical path ℓ = 1.40 cm, this value predicts (to within ~ 30%) a single-pass self-absorption loss of $(1-e^{-\varepsilon N \ell}) = 0.061$, which accounts for virtually all of the observed loss.

Knowledge of the laser cavity losses permits the calculation of the optimum output coupling, following the theory presented by Siegman . Based upon a threshold of 230J with the $\delta_e = 0.18$ output mirror, the minimum possible threshold, obtained with $\delta_e = 0$, would be E_{po} = 108.8 J. The optimum output coupling for pumping at 500 J is then δ_e (optimum) = δ_o [E_p/E_{po} - 1] = 0.159, which is so close to the 18% coupling of the present output mirror that the output power we obtained is within 1% of that which would be obtained with the exact optimum coupling.

This technique for determining the cavity losses also permits evaluation at two points of the small-signal gross gain coefficient g_o as a function of flashlamp energy, since at threshold gain equals loss. We distinguish gross gain g_o, defined on a single-pass basis by I_{out} (pumped)/I_{out} (unpumped) = $e^{g_o \ell}$, from net gain $(g_o - \alpha_o)$, defined for a single pass by $I_{out}/I_{in} = e^{(g_o-\alpha_o)\ell}$, where $\alpha_o \ell$ = 0.072 is the loss measured above. The measured data for $g_o \ell$, presented in Fig. 7, lie very close to a straight line passing through the origin, as expected. Thus, from Fig. 7, the gain coefficient at 500 J is 0.226 cm^{-1} and the net single-pass gain of the DZZ-FPL is $e^{(g_o \ell - \alpha_o \ell)}-1 = 0.276$. This measured gain coefficient will be compared with theory in a later section; we now present the results of a single-pass amplifier experiment to verify the gain value.

The single-pass gain of the DZZ-FPL was measured by its amplification of the low-power signal from another flashlamp-pumped dye laser. This technique suffers from many experimental difficulties and inaccuracies, so only qualitative agreement with the above results was obtained. The flashlamp pulse for the probe laser was about 10 μsec long and timed to coincide with the DZZ-FPL flashlamp pulse (separate spark gaps for the two DZZ-FPL lamps were required in order to achieve consistent timing). Due to the low output power of the probe laser in comparison with the DZZ-FPL fluorescence, it was convenient to detect the output signal through a narrow-band interference filter, with the probe laser narrowed and tuned to the filter passband by a reflection grating. Even then DZZ-FPL

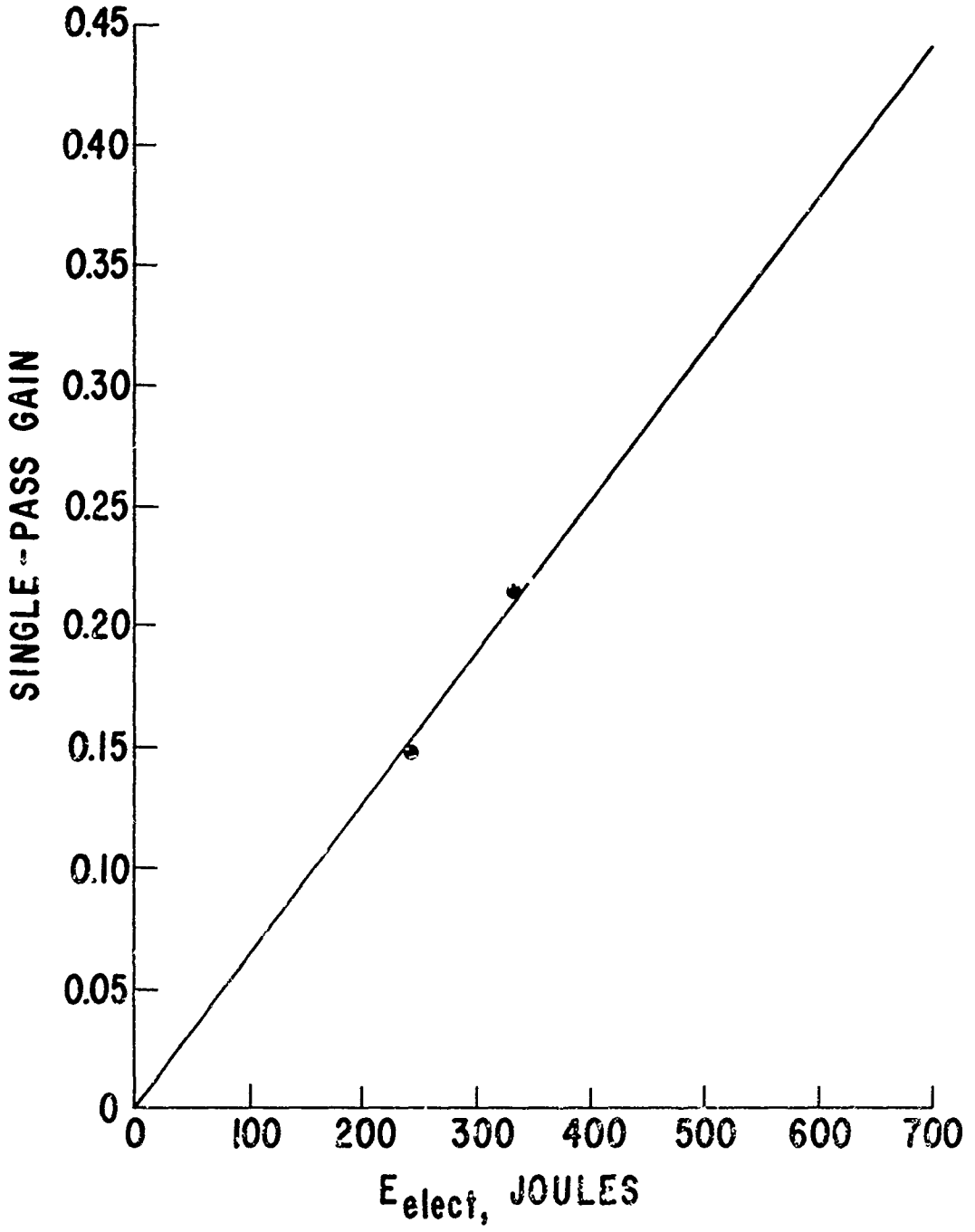

Fig. 7 Single-pass gain of DZZ-FPL as a function of input energy. The points shown were derived from oscillator thresholds with varying cavity loss.

fluorescence represented typically 30% of the output signal, and amplitude instability between pulses greatly complicated the data. The data taken at 500 J indicated that $g_o \ell$ is probably about 0.3 but certainly within the range between 0.15 + 0.50, as compared with the value obtained from the oscillator measurements of $g_o \ell = 0.315$. Although further refinement of the experimental apparatus could provide higher accuracy, these results were considered adequate confirmation of the small-signal gain measured as an oscillator.

C. Oscillator Beam Size and Divergence

The laser beam emanating from the DZZ-FPL oscillator, in the same configuration as discussed in the previous section, was examined within the range of input energy that corresponded to linearly increasing output ($\sim$ 100 mJ) where the laser beam size appeared to fairly constant. The laser beam size and shape in the near field were studied by photographing the graph paper upon which the beam was incident with varying attenuation in front of the camera. The power in each laser pulse photographed was monitored and only those shots with the same output power were compared. Unless the saturation behavior of the film is well known, a densitometer trace of a supposedly unsaturated single-pulse pattern is unreliable. Assuming that the saturation intensity is constant for the Polaroid Type 107 film, the edge of saturation represents a contour of constant intensity which can be compared with similar contours on photographs taken with more or less attenuation. These contours are shown in Fig. 8, where only the relative values of the contours are meaningful.

As can be seen from Fig. 8, the laser beam shape is fairly radially symmetric. Furthermore, if the relative intensity is plotted versus distance along the vertical cross-section shown, the radial variation of the intensity closely matches a Gaussian, $I(r) = I_o \exp(-2r^2/w^2)$, with w = 1.24 cm providing the best fit. Thus, 80% of the energy lies within a circle of diameter 2.22 cm. The usual criterion for a Gaussian beam to "fill" a laser medium is that $w \approx D/3$; for the DZZ-FPL with D = 3 cm that criterion is well satisfied. [It should be emphasized that the DZZ-FPL output is not a single transverse (TEM_{00}) mode, which would have a Gaussian distribution with $w_o = 0.0581$ cm for this cavity, but consists of many transverse modes, on the order of $(1.24/0.0581)^2 = (21.3)^2 = 456$, whose superposition is approximately Gaussian.] Because the output spot is not a 3 cm square of constant intensity, some of the power present in the inversion is not being utilized, and the output efficiency is accordingly reduced by the ratio of the oscillating area to the total DZZ-FPL aperture:

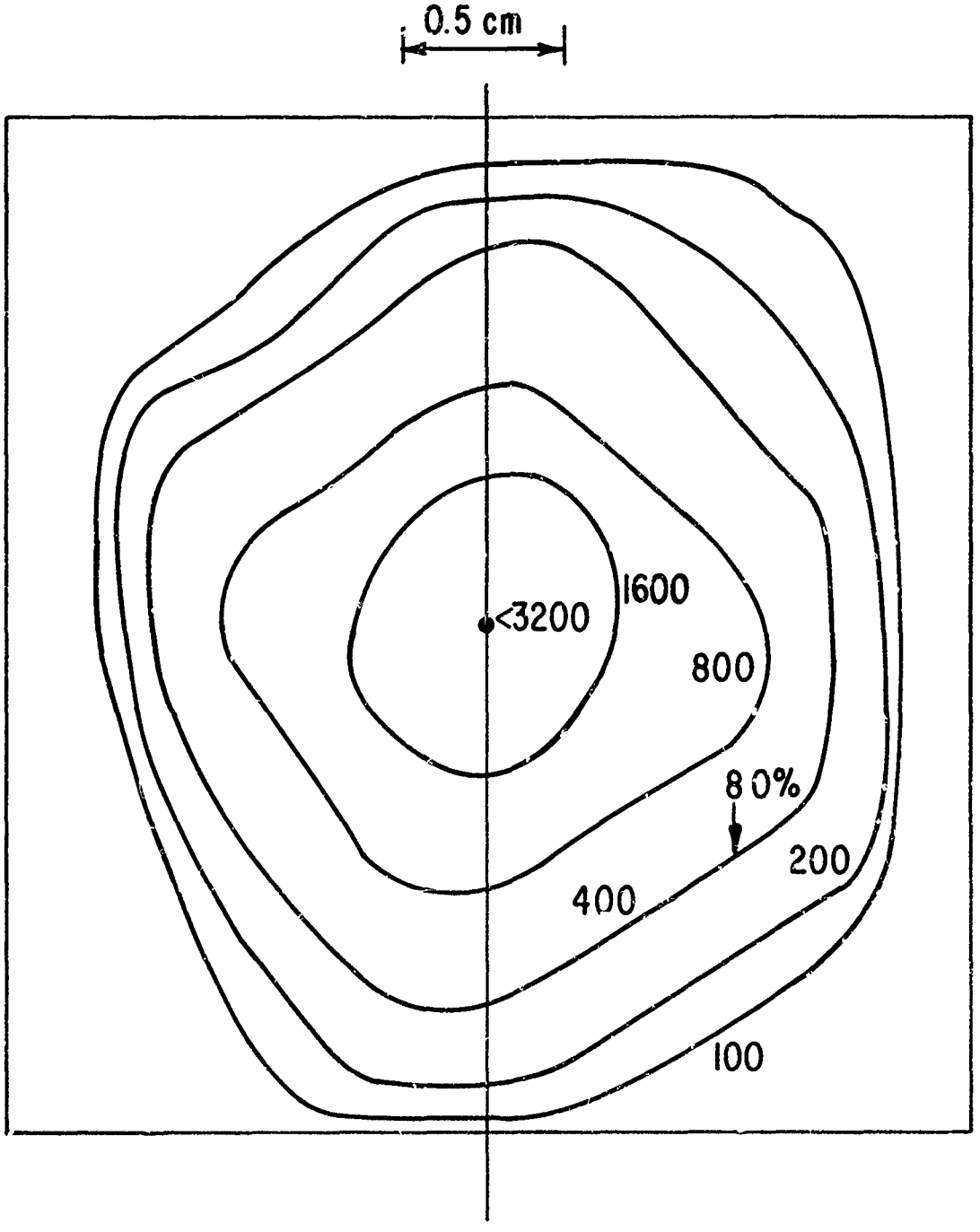

Fig. 8 Near-field intensity contours for DZZ-FPL oscillator.

81

$\eta_{ap} = (\pi w^2/2)/D^2 = 0.216$. The modes required to fill out the remainder of the square aperture apparently suffer too much diffraction loss to oscillate. The situation might be improved by using mirrors of larger aperture or longer radius of curvature or simply by pumping a smaller aperture DZZ-FPL.

The DZZ-FPL beam divergence was determined by passing the beam through a lens with a long focal length onto a graph-paper screen placed in the focal plane of the lens, as shown in Fig. 9, except that the microscope objective was not needed for magnifying the image. The pattern in this focal plane represents the far-field propagation angles according to $r = f_1 \theta$, as can be shown rigorously both for a TEM_{00} mode and for a plane wave through a circular aperture (Airy pattern). The divergence pattern was photographed with varying attenuation before the camera, and the output power monitored as in the previous measurement of beam size. The divergence pattern was radially symmetric to about the same degree as the near-field pattern (see Fig. 8). About 80% of the laser power was contained within a circle of diameter 1.8 cm; therefore 80% of the laser power is emitted into far-field divergence half-angles (measured from the optical axis to the direction of propagation) of 7.4 mrad. One way of viewing this result is to compare it with the far-field diffraction angle of a TEM_{00} mode of the same spot size at its waist, in this case $w_o = 1.24$ cm, for which $\theta = \lambda_o/\pi w_o = 0.0153$ mrad; the DZZ-FPL oscillator accordingly operates at 480 times "diffraction-limit". A second interpretation is to compare it with the far-field divergence angle of the TEM_{00} mode for this oscillator cavity, which is 0.326 mrad, so we can loosely say that there are about $(7.4/0.326)^2 = (22.7)^2$ 515 transverse modes oscillating; this result agrees well with a similar comparison between near-field spot sizes that suggests 456 transverse modes, as discussed above.

82

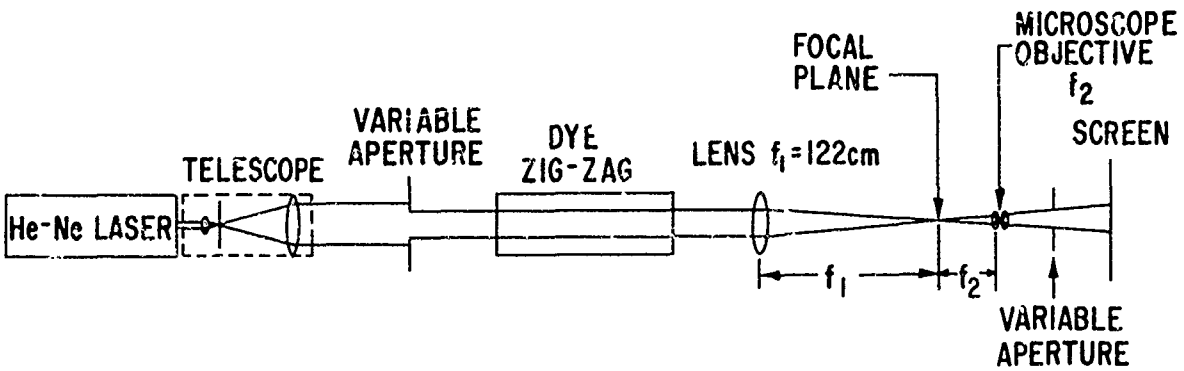

Fig. 9 Apparatus for measuring beam divergence and optical distortion.

IV. DZZ-FPL OPTICAL DISTORTION IN REPETITIVELY PULSED OPERATION

The principal advantage of the dye Zig-Zag-FPL configuration over the conventional cylindrical dye cell configuration is the expected large reduction of optical beam distortion even at moderate repetition rates ($\sim$ 10 pps). The reduction of distortion is due to two inherent features of the DZZ-FPL. First, the optical configuration plus the uniform face pumping ensure that thermal heating and optical gain are uniform over the aperture during each pulse. Thus each ray propagating parallel to the optical axis sees the same optical and thermal environment. Second, the optical configuration also leads to partial self-canceling of cumulative thermal effects of previous pulses. That the thermal effects largely cancel during a pulse is demonstrated by the absence of any distortion for about the first twenty pulses when the DZZ-FPL is operated with the dye solution not flowing. Nor could any distortion be observed when the DZZ-FPL was operated at 2 pps for several minutes with the solution flowing. The only thermal effect which was observed is a distortion during the interval between pulses when the dye solution heated by the pulse is being replaced by cool dye solution. Operation during the dye-exchange period would have considerable distortion. At the present dye flow rate this puts a limit on the pulse rate of about 7 pps.

The optical beam distortion properties of the DZZ-FPL were examined using an expanded collimated He-Ne laser beam at 633 nm. For these measurements the DZZ-FPL operated with 500 joules into the flashlamps at repetition rates up to 2 pps, the highest repetition rate for which the flashlamps and spark gaps then in place would fire consistently. The output beam of the Spectra-Physics Model 120 He-Ne laser was checked to be single-mode (TEM_{00}). This beam was focused, spatially filtered through a 6.8 μm-diameter aperture, expanded, and collimated by a commercial Spectra-Physics telescope. After being stopped down by a variable aperture, the beam traversed the DZZ-FPL along its optical axis. No distortion, such as thermal lensing, was observed in the near-field pattern projected on a screen a short distance after the DZZ-FPL for any repetition rate up to 2 pps for operating periods up to 5 minutes.

The far-field diffraction pattern was examined using the apparatus shown in Fig. 9. The far-field pattern, which appears in the focal plane of the first lens, is magnified by the microscope objective and projected on a screen. For collimated light incident upon the first aperture, this pattern is the familiar

Airy pattern, consisting of rings surrounding a central bright disk of radius (to the first minimum) $R = \theta f_1 M = (1.22 \lambda/d) f_1 M$, where θ is the beam-divergence half-angle, M is the magnification due to the microscope objective, and d is the diameter of the first aperture. In practice, the diameter of the first aperture had to be $d \leq 0.6$ cm to prevent distortion of the Airy pattern into a cross due to aberrations in the telescope. With this setup, any thermal distortion by the DZZ-FPL would change the size or shape of the central Airy disk.

With the DZZ-FPL firing, the only change in the Airy pattern that could be seen visually was a very faint upward (in the direction of the fluid flow) bouncing of the entire pattern on each pulse. This bouncing was independent of repetition rate and proportional to lamp energy. It could be eliminated by blocking the pump light from the lamps. During the flashlamp pulse the temperature of the dye within the channels increases nearly uniformly due to the nonradiative energy transitions. Then the dye flow forces fresh cool dye into the channels from the reservoir below, leading to a vertical variation of dye temperature within the channel. Since the index of refraction of ethanol has a negative temperature coefficient, He-Ne rays traversing the warmer dye near the top of the DZZ-FPL travel faster than those near the bottom, so that the phase-front is tilted downward. The direction of the bounce is inverted by the microscope objective and appears as an upward deflection of the Airy pattern. The magnitude of the observed deflection was measured to be $\sim 1.35 \times 10^{-5}$ radian. Since the bouncing is caused by the dye flow, it should disappear when the dye flow is stopped, as was experimentally verified. (With no dye flow the only distortion is thermal cylindrical lensing which sets in after $\sim$ 20 pulses at 1 pps.) The time behavior of the bouncing was observed by placing a small-aperture photodiode at the 12 o'clock minimum of the Airy pattern. The signal that was observed became noticeable about 40 msec after the flashlamp pulse, grew in intensity for 40-60 msec and disappeared about 140 msec after the flashlamp pulse. The total duration of 140 msec correlates well with the independently measured dye pumping rate which produces dye exchange in 130 msec. It must be emphasized that for repetition rates below the reciprocal of the dye-exchange time, i.e., below 7 pps, the bouncing distortion in no way affects the operation of the DZZ either as an oscillator or as an amplifier, since the optical pulse is completed long before the distortion becomes appreciable. The limit this

V. REPETITIVELY PULSED ONE-WATT DZZ-FPL OSCILLATOR

Based upon our earlier measurements of single-pulse oscillator output power and of the absence of distortion at a repetition rate of 2 pps, we might expect, and we have achieved, average power output in the vicinity of 1W for a repetitively pulsed DZZ-FPL oscillator. For this demonstration we installed new flashlamps, cleaned all the optical surfaces, and cleaned the single sparkgap used for triggering the flashlamps. With only one sparkgap, the highest repetition rate at which consistent triggering could be obtained was 3 pps. A CRL Model 205 Thermopile Power Meter monitored the average output power of the DZZ-FPL oscillator as the flashlamp power supply voltage was slowly increased. The output power was quite stable at any supply setting and rose quite smoothly as the flashlamp energy was increased, up to an output power level of 1.05 W, at which point the sparkgap began to self-trigger. The energy into the flashlamps at the 1W output power level was about 600 J. Extrapolating the data of Fig. 6 to 600 J input, we would expect about 300 mJ output in a single pulse. Thus our measurement of this same output energy per pulse when operating at a repetition rate of 3 pps is a strong indication of the lack of distortion with the DZZ-FPL. We observed operation at the 1W level for about a minute, but we could reasonably expect 1W operation for the entire lifetime of the flashlamps, about 10^4 to 10^5 pulses, or about 1 to 10 hours at 3 pps.

V. REPETITIVELY PULSED ONE-WATT DZZ-FPL OSCILLATOR

Based upon our earlier measurements of single-pulse oscillator output power and of the absence of distortion at a repetition rate of 2 pps, we might expect, and we have achieved, average power output in the vicinity of 1W for a repetitively pulsed DZZ-FPL oscillator. For this demonstration we installed new flashlamps, cleaned all the optical surfaces, and cleaned the single sparkgap used for triggering the flashlamps. With only one sparkgap, the highest repetition rate at which consistent triggering could be obtained was 3 pps. A CRL Model 205 Thermopile Power Meter monitored the average output power of the DZZ-FPL oscillator as the flashlamp power supply voltage was slowly increased. The output power was quite stable at any supply setting and rose quite smoothly as the flashlamp energy was increased, up to an output power level of 1.05 W, at which point the sparkgap began to self-trigger. The energy into the flashlamps at the 1W output power level was about 600 J. Extrapolating the data of Fig. 6 to 600 J input, we would expect about 300 mJ output in a single pulse. Thus our measurement of this same output energy per pulse when operating at a repetition rate of 3 pps is a strong indication of the lack of distortion with the DZZ-FPL. We observed operation at the 1W level for about a minute, but we could reasonably expect 1W operation for the entire lifetime of the flashlamps, about 10^4 to 10^5 pulses, or about 1 to 10 hours at 3 pps.

VI. PERFORMANCE ANALYSIS

In this section we present theoretical expressions for gain and efficiency applicable to the DZZ-FPL configuration, and make comparisons with our experimental results. A gain expression derived from fundamental laser principles indicates how device performance scales with various DZZ-FPL parameters. When compared with our measured gain, it provides information on the inversion efficiency (the power available in the inversion divided by the electrical power into the flashlamps), as does the experimentally determined slope efficiency. Performance of the DZZ-FPL as a large-signal amplifier is projected on the basis of measured efficiency and a theoretical expression that includes the effects of saturation and absorption. These results form the basis for the recommendations of the next section.

First we define symbols representing the geometry of the DZZ-FPL, with reference to Fig. 1. Let n be the number of dye channels (n = 10 in the experimental DZZ-FPL). The (n-1) clear 45°-45°-90° prisms have height (in the plane of the flashlamps) D, base 2D, and thickness (normal to the flashlamp plane) W, with D = W = 3 cm in the experimental DZZ-FPL. The dye channel spacing, normal to the prism surfaces, is g, with an optimum g = 0.91 mm determined for our DZZ-FPL. Since the dye/ethanol solution nearly index-matches the fused silica prisms, refraction in the channels can be neglected, so the paths for the pump light and for the laser light in each dye channel are nearly orthogonal and of equal length, approximately $\sqrt{2}g$. The lamp length L must overlap all the dye channels, so $L = n\ (D + \sqrt{2}g) \approx nD$, with L = 30 cm for the experimental DZZ-FPL. The laser path length through all channels is $\ell = \sqrt{2}gL/(D+\sqrt{2}g) \approx \sqrt{2}\ gL/D$; with refraction included it is actually about 8% longer, or ℓ = 1.40 cm for the experimental DZZ-FPL. The total dye volume in the channels is $V = \sqrt{2}\ gWDL/(D+\sqrt{2}g) \approx \sqrt{2}g\ WL$; $V = 11.65\ cm^3$ for the experimental DZZ-FPL.

In this analysis we can assume uniform pumping and hence uniform inversion with complete confidence. With the conventional cylindrical geometry, uniform pumping is a poor assumption for a system that makes efficient use of its pump light, i.e., radius comparable to the 1/e absorption length. The inversion density across each dye channel of the DZZ-FPL is also not uniform, but no matter what the true inversion profile is, the symmetry of the face-pumped laser causes the gain through each channel experienced by each ray propagating parallel to the optical axis to be identical to the gain through a uniformly

inverted channel. That is, there is no experiment which can differentiate between uniform inversion and the true inversion profile of the DZZ-FPL. Furthermore, this gain is constant across the entire DZZ-FPL aperture, as was demonstrated by Martin and Almasi[4] with the Nd:glass Zig-Zag-FPL.

With uniform inversion density in the dye channels, the inversion efficiency is given according to its definition by

$$\eta_{inv} = \frac{h\nu_o \; V \; \Delta N/\tau}{P_{elect}}$$

where ν_o is the frequency of oscillation, ΔN is the inversion density, τ is the lifetime of the upper laser state, and P_{elect} is the electrical power flowing into the flashlamps. The inversion efficiency is the product of several component efficiencies, each corresponding to a step in attaining the inversion:

$$\eta_{inv} = \eta_{lamp} \; \eta_{spectral} \; \eta_{pumping} \; \eta_{shift}$$

where: η_{lamp} is the efficiency of the flashlamp in converting electrical power from the power supply into light; $\eta_{spectral}$ is the fraction of light from the flashlamp that falls within the dye's absorption bands; $\eta_{pumping}$ is the fraction of spectrally useful light that is actually absorbed in the dye channels, and is determined by the geometrical arrangement of dye, flashlamps, and reflections; η_{shift} is the ratio of the laser frequency to the average pumping frequency. In the analysis that follows, estimates for η_{inv} will be obtained from our gain and slope efficiency measurements. However, two of its components $\eta_{spectral}$ and η_{shift} can be readily evaluated.

From the absorption spectrum for Rhodamine 6G in ethanol published by Snavely[2], the mean wavelength of absorption is 509 nm, so for oscillation at 595 nm, $\eta_{shift} \approx 0.855$. The spectral efficiency can be calculated from this absorption spectrum, dye concentration, channel thickness, and knowledge of the spectral output of the lamps. At these high current levels the spectral output has been found to be approximately black-body radiation from a color temperature determined by the current density, $T = K J^{\frac{1}{4}}$. For our lamps we calculate $T \approx 1.1 \times 10^4$ K, resulting finally in $\eta_{spectral} \approx 0.12$.

The net gain of a single-pass laser amplifier is given, as discussed in an earlier section, by $I_{out}/I_{in} = \exp[(g_o - \alpha_o)\ell]$. By convention the emission cross-

section σ_e is then defined by $g_o = \sigma_e \Delta N$. Unfortunately, in relating the emission cross-section (and the saturation parameter, which will be of interest shortly) to observable parameters of the laser medium, one can consult N authorities and, after sorting out the N different terminologies, arrive at N different results, differing by factors of 2, π, n^3 (index of refraction), etc. Having derived it rigorously and having checked its agreement with the most trustworthy authorities, we submit the following expression for emission cross-section:

$$\sigma_e = \frac{\lambda_o^4}{4\pi^2 n^2 c \Delta\lambda \tau_{rad}} \qquad \text{for the center of a Lorentzian lineshape}$$

$$= \frac{\lambda_o^4 E(\lambda_o)}{8\pi n^2 c \tau} \qquad \text{for a dye laser with } \int_o^\infty E(\lambda)d\lambda = \emptyset$$

where λ_o is the wavelength of oscillation, $\Delta\lambda$ the half-power linewidth of the fluorescence, and $\tau_{rad} = \tau/\emptyset$, where $\emptyset$ is the quantum efficiency. The line-shape factor $E(\lambda)$ was determined experimentally by Snavely[2] for Rhodamine 6G in ethanol, with $E(595\text{ nm}) = 4.55 \times 10^6\ m^{-1}$. Therefore the gain coefficient for the DZZ-FPL configuration is

$$g_o = \sigma_e \Delta N = \frac{\lambda_o^5 E(\lambda_o)\ \eta_{inv}\ P_{elect}}{8\pi n^2 c^2 h V} = \frac{\lambda_o^5 E(\lambda_o)\ \eta_{inv}\ P_{elect}}{8\pi n^2 c^2 h\ (\sqrt{2}gWL)}$$

We note also that the single-pass gain factor, $g_o\ell$, is independent of g and L:

$$g_o\ell = \frac{\lambda_o^5 E(\lambda_o)\ \eta_{inv}\ P_{elect}}{8\pi n^2 c^2 h W D}$$

We now compare this expression for the gain coefficient with the experimentally measured gain, $g_o = 0.226\ cm^{-1}$. With 500 J into the lamps in an 8 μsec pulse, P_{elect} (peak) $= 6.25 \times 10^7$ W. The index of refraction of ethanol is n = 1.36, and the wavelength was $\lambda_o = 595$ nm. Therefore, to achieve $g_o = 0.226\ cm^{-1}$ with this system implies $\eta_{inv} = 0.0345$ (3.45%), which is a quite reasonable value.

The slope efficiency of a laser oscillator is also related to the inversion efficiency. A flashlamp-pumped dye laser, for which the upper-state lifetime of 5 nsec is much shorter than the flashlamp pulse-width of 10 μsec, is actually operating quasi-cw, so the relevant slope efficiency relates the laser peak output power to the peak electrical power P_{elect}. This instantaneous slope efficiency for the experimental DZZ-FPL is 0.123%. It is related to the inversion efficiency according to

$$\eta_{slope} = \eta_{inv}\,\eta_{output}\,\eta_{aperture}$$

where η_{output}, the ratio of output coupling cavity loss to total cavity loss, equals 0.564 and $\eta_{aperture}$, the ratio of the oscillating area to the total DZZ-FPL aperture, equals 0.216 as discussed in the section on oscillator beam size. These values then imply that $\eta_{inv} = 0.0101$ (1.01%). The rather large discrepancy between the inversion efficiency values indicated by these two measurements may be due to the different laser operating conditions under which these measurements were made, such as a shift in oscillation wavelength between threshold and the linear region, or perhaps multi-mode complications that this theory does not account for. On the other hand, some of the discrepancy may be simply experimental inaccuracy; for example, a shift in oscillation wavelength of only 10 nm changes $E(\lambda)$ by nearly a factor of 2. At any rate, the true value for the inversion efficiency is somewhere between these values, probably near 2%. According to the earlier discussion about the components of the inversion efficiency, we therefore may infer that $\eta_{lamp}\,\eta_{pumping} \approx 0.20$, which is a reasonable value considering that most flashlamps are about 50% efficient and pumping cavities are typically 40-60% efficient.

The DZZ-FPL is expected to be used primarily as a large-aperture low-distortion amplifier. The low small-signal gain of the present unit discourages its use as a small-signal amplifier; for this application a conventional cylindrical dye amplifier or a scaled-down version of the DZZ-FPL, as will be discussed in the next section, would be more appropriate. But as a large-signal amplifier the DZZ-FPL could add several joules of energy to a dye laser pulse with high efficiency. Here we present theoretical predictions for the operation of the DZZ-FPL as a large signal amplifier, with gain saturation and loss taken into account.

Our analysis for a single-pass traveling-wave amplifier closely follows that of Pantell[5], except that we consider a four-level atomic medium. The result of this analysis is a differential equation for the light intensity as a function of z, the distance along the optical axis from the entrance plane:

$$\frac{dI}{dz} + \alpha_o I = \frac{\sigma_e(\lambda)}{1+I/I_{sat}(\lambda)} \Delta N \, I$$

where $\sigma_e(\lambda) = \frac{\lambda^4 E(\lambda)}{8\pi n^2 c \tau}$

and $I_{sat}(\lambda) = \frac{h c}{\lambda \tau \sigma_e(\lambda)}$

This equation reduces to the conventional gain expression considered earlier when $I \ll I_{sat}$. The solution of this equation for I(z) is a transcendental expression that can only be evaluated numerically:

$$\ln \frac{I(z)}{I(0)} + p \ln \left(\frac{p - 1 - I(0)/I_{sat}}{p - 1 - I(z)/I_{sat}} \right) = (p-1)\alpha_o z$$

where $p = \frac{g_o}{\alpha_o} = \frac{\eta_{inv} P_{elect}}{\alpha_o \ell_{WD} I_{sat}}$ is the pumping parameter.

Figure 10 shows the growth of the optical beam for various input intensity levels as it propagates along a DZZ-FPL amplifier characterized by the same loss coefficient ($\alpha_o = 0.06$ cm^{-1}) and pump power per unit length (p = 3.80) as our experimental DZZ-FPL operating at 500 J and λ = 595 nm. The output intensity from an infinitely long amplifier with constant pump power per unit length (which would, of course, require infinite electrical power), or equivalently from a large number of identical amplifiers in cascade, does not approach infinity, but approaches a finite limiting intensity $I(\infty) = I_{sat}(p-1)$, due to the effects of saturation in reducing the gain to where it just balances the loss. The optical path length of the experimental DZZ-FPL, indicated at ℓ = 1.4 cm, is considerably shorter than the distance at which saturation is approached for $I(0)/I_{sat} \ll 1$, as expected due to the low gain of the experimental version. Therefore its

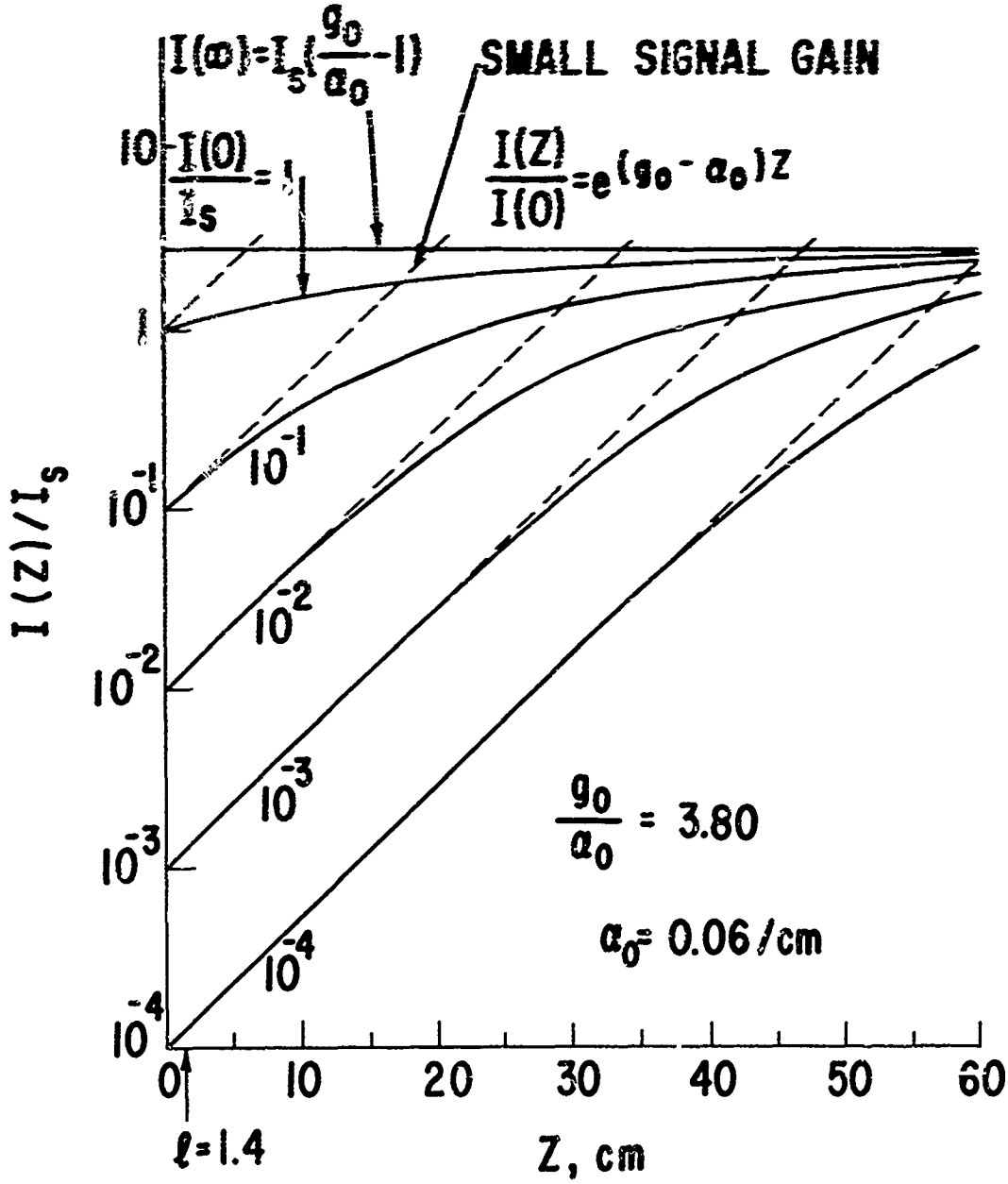

Fig. 10 Single-pass laser amplification including the effects of saturation and loss, showing intensity versus length for various incident intensities.

efficiency as an amplifier, given by

$$\eta_{amp} = \frac{\Delta E(L)-E(0)}{E_{elect}} = \eta_{inv} \frac{E(L)/E_{sat}-E(0)/E_{sat}}{gL}$$

is quite low until $E(0)/E_{sat} \lesssim 1$, as plotted in Fig. 11. Amplifier efficiency can never be greater than the inversion efficiency, and only with high gain (large g) does it approach this limit.

For our numerical example at λ = 595 nm, with τ = 5.5 msec, σ_e(595 nm) = 7.43×10^{-17} cm^2 and I_{sat} (595 nm) = 0.82 MW/cm^2. With the 5 μsec long output from the flashlamp-pumped oscillator or preamplifier expanded to 9 cm^2 area, our DZZ-FPL amplifier would require for efficient operation $I(0) = I_{sat}$ or $E(0)$ = 36.8 J; at this level is would add 2.8 J to the pulse. From the efficiency curve of Fig. 11 this DZZ-FPL can still add 1.4 J to the pulse for input as low as $E(0)$ = 7 J. Thus, owing to the high saturation intensity of dye lasers and to the large aperture and low gain of the present DZZ-FPL, its use as an amplifier is probably limited to high input energy applications. In the concluding section we will discuss alternative DZZ-FPL configurations which extend its usefulness as an amplifier at low input energies.

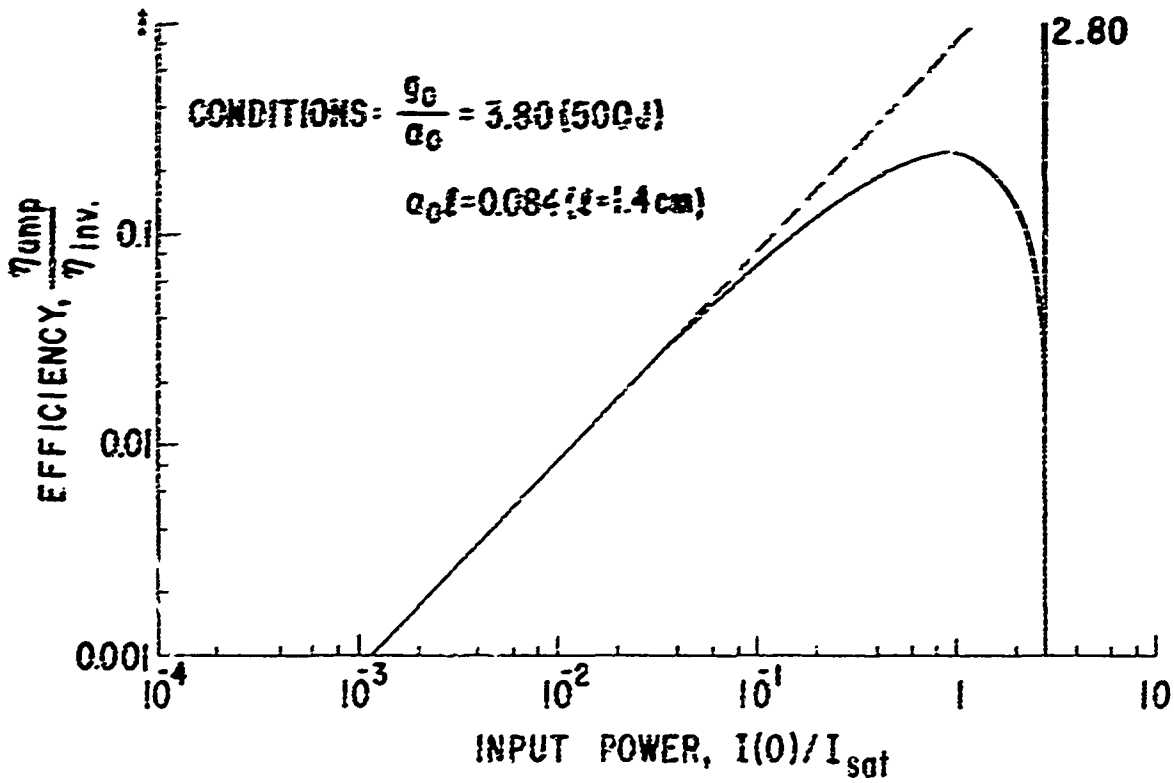

Fig. 11 DZZ-FPL amplifier efficiency, normalized to inversion efficiency, as a function of incident intensity.

VII. CONCLUSIONS AND RECOMMENDATIONS

In this work we have demonstrated the operation of the dye Zig-Zag-Face-Pumped Laser. The operating parameters of the device constructed were optimized under single-pulse operation as a laser oscillator. The gain, loss, and output power characteristics of the DZZ-FPL oscillator were measured and correlated with theoretical expectations. No long-term optical distortion was observed when the unit operated at 2 pps for several minutes. The only visible distortion occurred after each laser pulse while the dye in the channels was being replaced; the repetition rate limit thereby imposed can be raised by increasing the dye flow rate. The small-signal gain performance of the DZZ-FPL as an amplifier was confirmed in a seperate experiment. Amplifier performance with signals approaching the saturation level and amplifier efficiency were analyzed. It is expected that the present DZZ-FPL is most useful as an amplifier when the input optical signal contains several joules of energy.

As recommendations for future work, we consider, with the aid of the theory of the previous section, the possibilities of alternative DZZ-FPL configurations that might be more useful as oscillators or low-level amplifiers. For both, it appears advantageous to reduce one or both dimensions of the aperture and to consider multiple passes. In particular, we consider three optical passes, each with a 1 x 1 cm aperture, through a DZZ-FPL with D = 1 cm and W = 3 cm (see Fig. 1) Since the area facing the flashlamps is the same as in the present 3 x 3 cm unit, the inversion efficiency η_{inv} is the same if the channel thickness and concentration are the same. Furthermore the gain coefficient g_o is the same for the same flashlamp power. However, reduction of D by 3 at constant L requires 3 times more channels (and 3 times more prisms); considering also the three-pass optical folding, the total increase in active dye length is a factor of 9.

As an oscillator this configuration would offer the following advantages:

- The smaller aperture and multiple passing should provide uniform intensity over the entire 1x1 cm^2 beam area, with $\eta_{aperture}$ thereby approaching unity and slope efficiency increasing accordingly;
- The longer active dye lergth should reduce threshold to the limit dictated by self-absorption losses ($\sim$ 130 J) and may permit larger output couplin.;

- Lower dye concentration might reduce self-absorption losses with little enough sacrifice in inversion efficiency to further reduce threshold and increase slope efficiency.

As a small-signal amplifier, the improvements are even more significant:

- The longer dye path length with the same gain and absorption coefficients should provide a substantial improvement in net small-signal gain, from $I_{out}/I_{in} = 1.276$ to $I_{out}/I_{in} = 8.30$ (9.2 db);
- The longer path length is also substantially closer to the length required for the output signal to be approaching the saturation limit, so that reasonable amplifier efficiency would be achieved with a lower input intensity ($I(0)/I_s \gtrsim 10^{-1}$) and the peak amplifier efficiency is higher;
- The 9 times lower beam area required for the input beam to this amplifier would also serve to reduce the input beam energy required for efficient operation, from 36.8 J to about 400 mJ when these latter two effects are considered. The combination of two of these 3-pass, 1x3 cm DZZ-PPL units, the first as an efficient oscillator with 400 mJ output, the second as an efficient medium-power amplifier capable of adding about 1.6 J to the pulse, would be an attractive package for producing 2 J tunable dye laser pulses at a repetition rate of 5 pps.

REFERENCES

1. Throughout this report, channel thicknesses are measured perpendicular to the prism surface. Since the optical axis is at 45° to this surface, the path through a channel along the axis is $\sqrt{2}$ times the channel thickness.

2. B.B. Snavely, Proc. IEEE, 57, 1374 (1969).

3. A.M. Siegman, An Introduction to Lasers and Masers, Sec. 10-6, McGraw-Hill (1971).

4. W.S. Martin and J.C. Almasi, G.E. Technical Report AFAL-TR-71-63 (1971).

5. R.H. Pantell and H.E. Puthoff, Fundamentals of Quantum Electronics, Sec. 3.4.1, John Wiley and Sons (1969).